



Thermochronologic constraints on evolution of the Linglong Metamorphic Core Complex and implications for gold mineralization: A case study from the Xiadian gold deposit, Jiaodong Peninsula, eastern China



Li-Qiang Yang^{a,*}, Jun Deng^a, Zhong-Liang Wang^a, Liang Zhang^{a,b}, Richard J. Goldfarb^{a,c}, Wan-Ming Yuan^a, Roberto F. Weinberg^b, Rui-Zhong Zhang^{a,d}

^a State Key Laboratory of Geological Processes and Mineral Resources, China University of Geosciences, Beijing 100083, China

^b School of Earth, Atmosphere and Environment, Monash University, Vic 3800, Australia

^c U. S. Geological Survey, Box 25046, Denver Federal Center, Denver, CO 80225, USA

^d Zhaoyuan Gold Mining Stock Co., Ltd., Zhaoyuan 265415, China

ARTICLE INFO

Article history:

Received 27 March 2015

Received in revised form 12 July 2015

Accepted 15 July 2015

Available online 17 July 2015

Keywords:

Fission track thermochronology

Gold mineralization

Linglong Metamorphic Core Complex

Xiadian gold deposit

Jiaodong Peninsula China

ABSTRACT

The NNE-trending Linglong Metamorphic Core Complex hosts the majority of the gold deposits in the Jiaodong Peninsula of eastern China. Many of the deposits are hosted by the 163–155 Ma Linglong granite in the footwall of the Linglong detachment fault. Argon thermochronology suggests that the granite had cooled to 400 °C by 143 ± 1.5 Ma possibly as a result of normal movement on the detachment. Nine zircon fission track (ZFT) ages from samples collected along a NW–SE transect perpendicular to the central part of the Linglong detachment fault at the –652 m level in the Xiadian deposit constrain the subsequent thermal evolution of Linglong Metamorphic Core Complex, which overlapped the period of major gold deposition.

The ZFT ages vary from 136.9 ± 3.3 Ma (1σ) to 130.1 ± 2.2 Ma (1σ). The unaltered Linglong granite in the footwall and amphibolite in the hangingwall have similar ages at 136.9 ± 3.3 Ma (1σ) and 135.0 ± 3.0 Ma (1σ), whereas ages for the disseminated- and stockwork-style ores appear to be younger at ca. 131–130 Ma, although there is an overlap of ages when considering the 1σ precision. Interestingly, ZFT ages show no marked differences between the hangingwall and footwall of the Linglong detachment fault, although significant movement along the fault occurred.

The results are best interpreted to indicate that the Linglong granite was emplaced at ~160 Ma, and cooled to 240 ± 50 °C at ~135 Ma, as recorded by unaltered rocks in the footwall. Hydrothermal alteration along the Linglong detachment fault led to annealing of zircon fission tracks and the consistent younger ages of ~131 Ma. Quartz aggregates associated with gold mineralization show evidence of recrystallization suggesting that the hydrothermal event was initiated at temperatures of at least 300–350 °C, near the brittle–ductile transition, but cooled rapidly to ZFT closure temperatures within a country-rock environment that was already relatively cool. Therefore these ZFT ages suggest that the timing of mineralization at the Xiadian deposit was post-135 Ma and likely very close to 131 Ma. The mineralization and cooling occurred in the footwall of a major detachment fault under an extensional regime, possibly related to the progressive slab rollback of the paleo-Pacific plate, and controlled by the Linglong Metamorphic Core Complex.

© 2015 Elsevier B.V. All rights reserved.

1. Introduction

Eastern Asia is characterized by widespread Late Jurassic to Early Cretaceous magmatic activity and continental extension (Daoudene et al., 2009; Charles et al., 2012) that led to the formation of NE–SW-

striking rift basins (Jahn et al., 2009; Wang et al., 2012; Daoudene et al., 2013; Fig. 1), scattered metamorphic core complexes (MCCs) (Davis et al., 2002; Liu et al., 2005; Mazukabzov et al., 2011; Wang et al., 2011; Ni et al., 2013; Fig. 1), and large-scale gold mineralization (Deng et al., 2003a,b, 2009; Goldfarb et al., 2014; Goldfarb and Santosh, 2014; Song et al., 2015; Fig. 1). Formation of most MCCs in Transbaikalia–northern Mongolia and northeastern China occurred in the Early Cretaceous (Donskaya et al., 2008; Lin et al., 2008). However, the development of the Linglong MCC in the Jiaodong Peninsula (Fig. 1), which was previously regarded as a group of sheared plutons,

* Corresponding author at: State Key Laboratory of Geological Processes and Mineral Resources, China University of Geosciences, 29# Xue-Yuan Road, Haidian District, Beijing 100083, China.

E-mail address: lqyang@cugb.edu.cn (L.-Q. Yang).

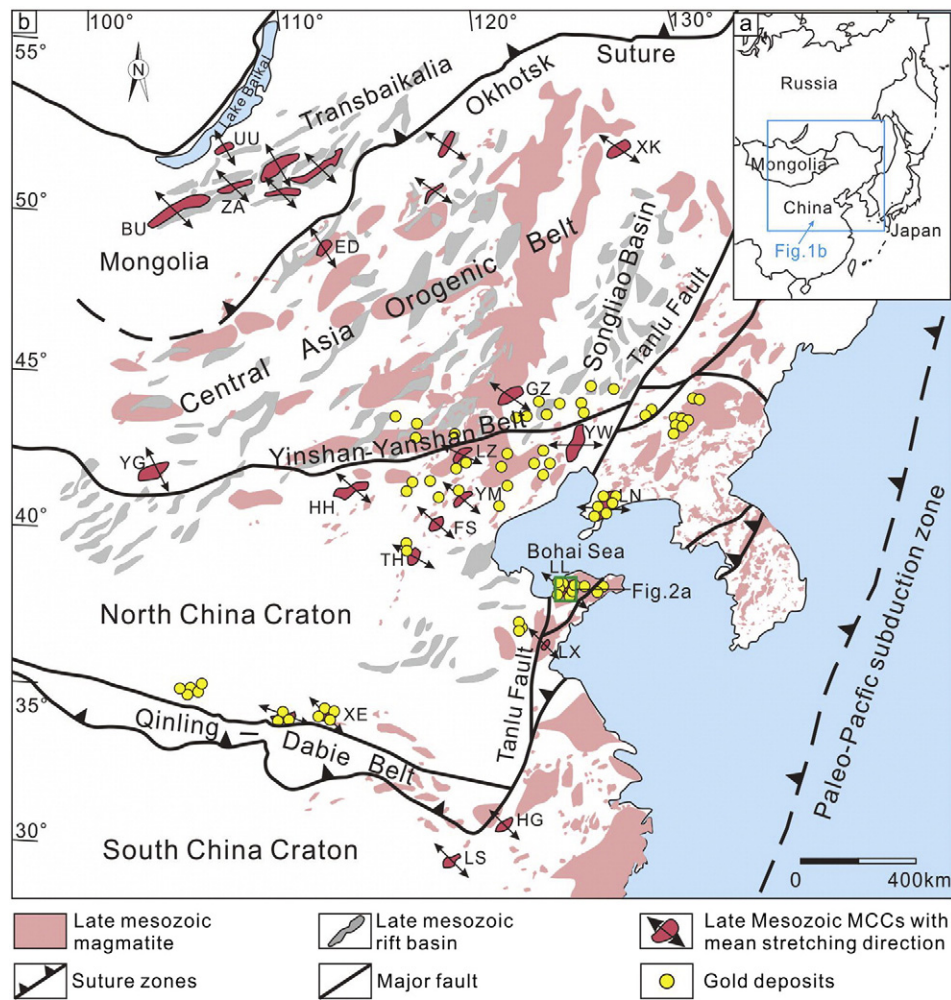


Fig. 1. Late Mesozoic extensional structures in eastern Asia (modified after Daoudene et al., 2013; Wang et al., 2012). Abbreviations for MCCs: BU, Buteel–Burgutoy; ED, Erendavaa; FS, Fangshan; GZ, Ganzhuermiao; HG, Hongzhen; HH, Hohhot; LN, Liaonan; LS, Lushan; LZ, Louzidian; LL, Linglong; LX, Luxi; TH, Taihang; UU, Ulan Ude; YW, Yiwulüshan; YG, Yagan; XK, Xinkailing; YM, Yunmeng Shan; and ZA, Zagan.

is now recognized to be older at ca. 160–150 Ma (Charles et al., 2013). Most importantly, the majority of gold resources in the Jiaodong Peninsula, the largest gold producing area in China with a proven reserve of >4000 t gold (Yang et al., 2014a,b), is hosted in the Linglong MCC (Wang et al., 2014, 2015; Yang et al., 2014c; Fig. 2a). Furthermore, a recent $^{40}\text{Ar}/^{39}\text{Ar}$ geochronological study of sericite and muscovite from the ores in the Dayingezhuang deposit (Fig. 2a), a large (>120 t Au) gold deposit occurring along the Linglong detachment fault on the eastern margin of the Linglong MCC, indicated that the earliest significant gold event took place at 130 ± 4 Ma in the Jiaodong Gold Province and may be related to evolution of the Linglong MCC (Yang et al., 2014c). However, the cooling and exhumation history of the Linglong MCC and the relationship between its evolution and gold genesis in the Jiaodong Peninsula are still poorly constrained. Accordingly, the crustal dynamic processes that led to large-scale gold mineralization in the Jiaodong Peninsula remain equivocal and contentious.

The >200 t Au Xiadian gold deposit, which is located 15 km to the southwest of the Dayingezhuang deposit (Fig. 2a), is situated in the central part of the Linglong detachment fault that defines the eastern edge of the Linglong MCC. The deposit provides excellent exposures of the hangingwall, footwall, and detachment itself, marked by mylonitic to ultramylonitic, cataclastic and brecciated rocks, and late brittle faults that are associated with well-developed silicification, sericitization, and sulfidation (Fig. 3a, b). It thus provides an ideal location to study the thermal evolution of the Linglong MCC, and associated ore-forming

activity. To date, no information on the geochronology of gold mineralization at Xiadian deposit has been published. A zircon fission track (ZFT) thermochronologic study has been undertaken here, examining the undeformed and deformed rocks of the Linglong MCC that are associated with the gold ores of the Xiadian deposit (Fig. 3b). Based on these new data, the relationship between gold mineralization and evolving continental dynamics of the Jiaodong area has been evaluated.

2. Geological setting

2.1. Linglong massif geology

The northwestern part of the Jiaodong Peninsula is dominated by the NNE-trending Linglong massif situated in the Pingdu–Laizhou–Zhaoyuan area (see “LL” on Fig. 2a; Deng et al., 2015a,b). The Linglong massif mainly consists of Mesozoic migmatitic and granitic rocks, which intruded the Late Archean and Paleoproterozoic rocks (Fig. 2). Recent study shows that the Linglong massif is an asymmetric MCC (Charles et al., 2013), comprising a footwall, separated from a hangingwall to the east, by a master detachment zone (Fig. 2), as detailed below.

The migmatites that are intercalated with isotropic granites constitute the footwall of the Linglong MCC (Sang, 1984; Fig. 2a). These granites yielded ages of 163–155 Ma (Ma et al., 2013; Yang et al., 2012) by U–Pb dating of zircons using laser ablation-inductively coupled plasma-mass spectrometry (LA-ICP-MS) and 143 ± 1.5 Ma by

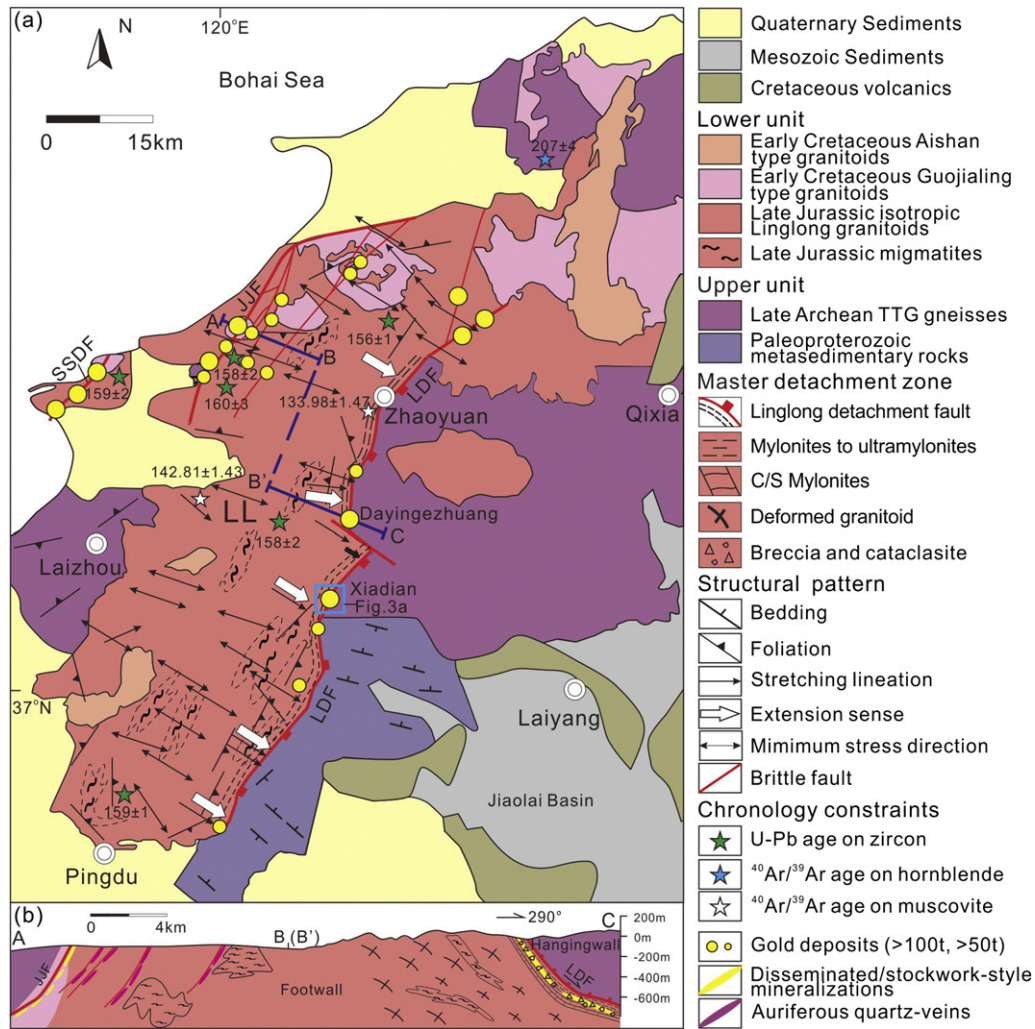


Fig. 2. (a) Simplified geological map of the Linglong Metamorphic Core Complex (modified after Charles et al., 2013). Profiles A–B and B'–C mark the line of cross-section in (b). U–Pb ages on zircon are from Ma et al. (2013) and Yang et al. (2012). $^{40}\text{Ar}/^{39}\text{Ar}$ ages on muscovite are from Charles et al. (2013). Amphibole $^{40}\text{Ar}/^{39}\text{Ar}$ age comes from Faure et al. (2003). (b) Schematic NW–SE section across the Linglong MCC (modified after Charles et al., 2011a). SSDF, Sanshandao Fault; JJF, Jiaojia Fault; LDF, Linglong detachment fault; LL, Linglong massif.

$^{40}\text{Ar}/^{39}\text{Ar}$ dating on magmatic muscovite (Charles et al., 2013). These ages are interpreted as the crystallization age of the melt and the granite cooling age through the closure temperatures of muscovite, respectively. Generally 400 ± 50 °C is accepted as the muscovite closure temperature for a relatively rapid cooling rate, and $360\text{--}350$ °C for a moderate cooling rate (Hames and Bowring, 1994; McDougall and Harrison, 1999; Harrison et al., 2009), with 270 °C commonly taken for slow cooling or extended reheating (Snee et al., 1988).

From the center to the eastern and southern margins of the massif, both the granitic and migmatitic rocks display progressively stronger finite strain, forming mylonitic to ultramylonitic rocks towards the top of the footwall (Fig. 2). The granites are characterized by the NE- and ENE-striking and E-dipping mylonitic foliation, and associated $120\text{--}140^\circ$ trending mineral and stretching lineations marked by biotite and quartz. Migmatitic fabrics along the eastern and southern borders strike roughly parallel to the foliation in the neighboring granite (Charles et al., 2011a; Fig. 2).

In the footwall, other granitoids have also been recognized. Within the northern part of the massif, the younger Guojialing-type granitoids are composed of porphyritic quartz monzonite, and granodiorite and monzogranite with large K-feldspar megacrysts (Hou et al., 2007; Zhang et al., 2010), and they intruded the Linglong migmatitic and granitic unit (Fig. 2a). These younger granitoids are characterized by sub-solidus deformation and well-developed C/S fabrics, and are considered

to be synkinematic intrusions (Charles et al., 2011a). Zircon U–Pb analyses yielded $132\text{--}123$ Ma crystallization ages for these plutons (Yang et al., 2012; Liu et al., 2014a,b; Wang et al., 2014). Moreover, the central, southwestern, and northeastern parts of the footwall were intruded by the Aishan-type granitoids, which are undeformed, post-tectonic bodies (Charles et al., 2011b). Crystallization of these plutons occurred at $118\text{--}110$ Ma, as shown by zircon U–Pb dating (Goss et al., 2010).

The hangingwall is composed of Late Archean tonalite–trondhjemite–granodiorite (TTG) gneisses and Paleoproterozoic metasedimentary rocks (Zhou et al., 2008; Deng et al., 2011; Zhai and Santosh, 2011). The TTG gneisses, exhibiting gneissic and migmatitic foliation, have protolith ages of $3.4\text{--}2.6$ Ga (Qiu, 1989; Wang et al., 1998), with amphibolite-to granulite-facies metamorphic ages of ca. 2.5 Ga (Jahn et al., 2008). The weakly deformed Paleoproterozoic metasedimentary rocks, lying unconformably on the TTG gneisses, comprise schists, paragneisses, calc-silicate rocks and marbles, with minor mafic granulite and amphibolite, and exhibit bedding that strikes oblique to the eastern border of the Linglong massif (Fig. 2a, Charles et al., 2011a).

The Linglong detachment fault is marked by a $030\text{--}040^\circ$ trending ductile shear zone with a width of ~ 4 km, including $\sim 0.5\text{--}1.0$ km of mylonitic–ultramylonitic rocks (Fig. 2). It is characterized by top-to-the-SE normal sense of shear (Fig. 2a), which combined with the consistent $120\text{--}140^\circ$ stretching direction in the footwall, indicates that the Linglong MCC was exhumed in a NW–SE-striking extensional regime.

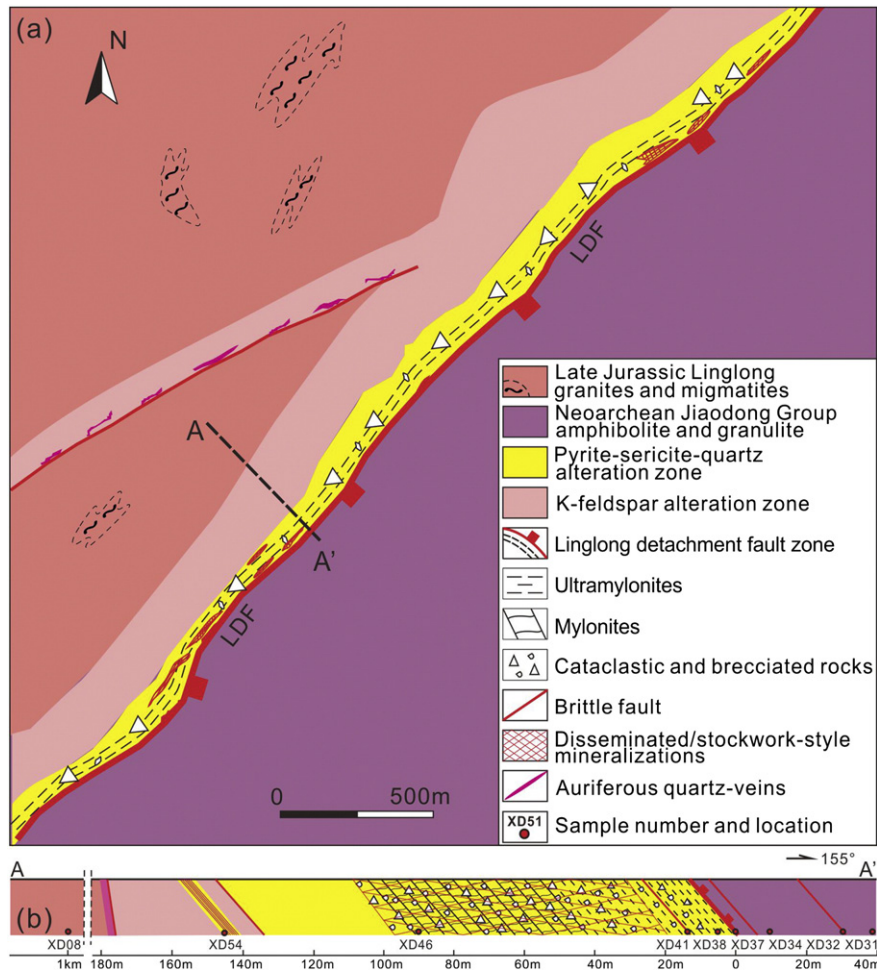


Fig. 3. (a) Simplified geological map of the Linglong detachment fault in the area of the Xiadian gold deposit. (b) Schematic NE-SW cross-section A-A' at the -652 m level of the Xiadian gold deposit showing the Linglong detachment fault (LDF) and sampling locations.

Secondary white mica from the mylonites in the detachment fault yielded a 134 ± 1.5 Ma $^{40}\text{Ar}/^{39}\text{Ar}$ age (Charles et al., 2013), interpreted as the age of ductile deformation along the detachment, which contrasts with the 143 ± 1.5 Ma age by $^{40}\text{Ar}/^{39}\text{Ar}$ on magmatic muscovite (Charles et al., 2013). Cataclastic and brecciated rocks are also observed along the detachment, which indicates that the fault was reworked under brittle conditions (Fig. 2b).

The Linglong MCC is bordered to the west by the 010–070°-trending Jiaojia fault zone, with a dip of 20–50° to the NW and a length of 60 km (Fig. 2). The fault zone is marked by cataclastic granitic rocks. Furthermore, all units of the Linglong MCC are affected by widespread, high-angle, small-scale faulting (Fig. 2). The K-feldspar, plagioclase, and quartz grains constituting the migmatites and the anatectic granites of the footwall are commonly cut by fractures and microfaults, indicating a superimposed brittle deformation (Charles et al., 2011a). These faults, which are particularly abundant in the footwall, mainly trend NE and show normal motion and form part of the overall NW–SE extensional event.

The Linglong MCC hosts the majority of the gold resources in the Jiaodong Peninsula (Wang et al., 2014, 2015). The gold deposits, typically hosted by the 163–155 Ma Linglong granite in the footwall of the Linglong detachment fault, are characterized by quartz vein mineralization and disseminations or quartz stockworks (Qiu et al., 2002; Deng et al., 2000, 2006, 2008; Yang et al., 2006, 2007a, 2008; Wen et al., 2015). The vein style of mineralization, such as that present at the Wang'ershan and Linglong deposits, is characterized by a series of sub-parallel NE-trending en-echelon auriferous veins that are controlled

by the high-angle, small-scale NE-trending faults within the Linglong MCC (Fig. 2). The disseminated- and stockwork-styles of mineralization, which characterizes the Jiaojia, Xincheng, Dayingezhuang, and Xiadian deposits, occurs along NE- to NNE-trending structures bordering the Linglong MCC (Fig. 2b).

2.2. Xiadian gold deposit geology

2.2.1. Alteration and gold mineralization

The Xiadian gold deposit, mainly characterized by disseminations and stockworks with less significant quartz vein mineralization, is hosted by the footwall granite and migmatite on the west side of the Linglong detachment fault (Fig. 2), and is thus below the Late Archean amphibolite and granulite in the barren hangingwall to the east (Fig. 3). The hydrothermal alteration at Xiadian includes sericitization, silicification, sulfidation, carbonation, and K-feldspathization, which are largely restricted to the Linglong detachment fault zone (Fig. 3). A K-feldspar alteration zone, with some of the K-feldspar clearly pre-dating the gold, extends for several hundred meters beyond the pyrite-sericite-quartz alteration (Fig. 3).

The less-common vein mineralization comprises a series of NE-trending en-echelon auriferous veins with surrounding vein-related pyrite-sericite-quartz altered rocks within the subsidiary faults, and this is mainly developed in the more K-feldspar-altered granite (Fig. 3). The occurrence of dynamically recrystallized quartz grains associated with gold-bearing pyrite in the pyrite-sericite-quartz altered

rock surrounding the veins (Fig. 4a, b) indicates early pyrite deposition at temperatures of at least ~300–350 °C (Passchier and Trouw, 2005).

The disseminated and stockwork-style orebodies, comprising a pyrite–sericite–quartz gold-bearing assemblage closest to the fault gouge and representing the main part of the resource, are associated with cataclasites and breccias. The minerals deposited with the gold are chiefly sericite, quartz, and pyrite (Fig. 4c), with trace amounts of chalcopyrite, galena, and sphalerite, indicating hydrothermal temperatures between 225 °C and 400 °C (McCuaig and Kerrich, 1998). Gold occurs mainly as non-refractory grains in microcracks within pyrite (Fig. 4d), closely associated with sericite grains, which together overprint the early dynamically recrystallized quartz veins (Fig. 4e). Thus they represent a relatively late, main gold-mineralization event associated with brittle deformation. The estimated ore-forming temperature based on fluid-inclusion studies is even narrower—240–300 °C—although there is a wide range of homogenization temperatures (140–380 °C) reported for the pyrite–sericite–quartz assemblage in the Xiadian gold deposit (Xu et al., 2013).

A fault gouge, 10–30 cm-thick, marks the last important cataclastic event along the Linglong detachment fault. It is related to small-scale, NE-trending high-angle normal faulting that occurred in both the altered granite and the Archean amphibolites. The fault gouge mainly consists of illite, montmorillonite, and kaolinite (Gao, 2008), indicating that it probably formed at temperatures below 240 °C (Zwingmann et al., 2010).

In summary, the temperature of hydrothermal alteration related to gold deposition in the Xiadian gold deposit is interpreted to be mainly

from 240 °C to 300 °C, with perhaps a slightly higher initial temperature for early pyrite. The fault gouge that marks the last main brittle movement along the Linglong detachment fault is considered to have formed at temperatures below 240 °C.

2.2.2. Deformation

Linglong granitic rocks hosting the ore at Xiadian underwent early mylonitization related to the exhumation of the footwall during normal movement along the detachment fault (Charles et al., 2013). These rocks have typical features of sheared granitic rocks, with sigma porphyroclasts of feldspars and garnets, and recrystallized quartz ribbons (Fig. 5a, b). Away from the mineralization, these rocks are reasonably fresh with only minor alteration, which includes minor calcite veins, minor pyrite in strain shadows, and rare sphalerite. Where rocks are more intensely altered, pyrite and sericite appear contemporaneous and help define the foliation. Pyrite, as aggregates forming lenses parallel to the foliation that have been stretched (Fig. 5c, d) and as folded aggregates, is interpreted to have been deposited during ductile deformation.

The most intensely altered rocks are complex breccias (Fig. 5e), with multiple fracturing and brecciation events leading to the physical and chemical breakdowns of the protolith. Clasts within the breccia of quartz aggregates, possibly representing early quartz veins, record ductile recrystallization. These clasts are embedded in a matrix of fine quartz, feldspar, sericite, and calcite, showing that the early silica alteration was ductile and was followed by brittle cataclasis forming the breccia. Locally, however, this fine matrix also shows signs of ductile

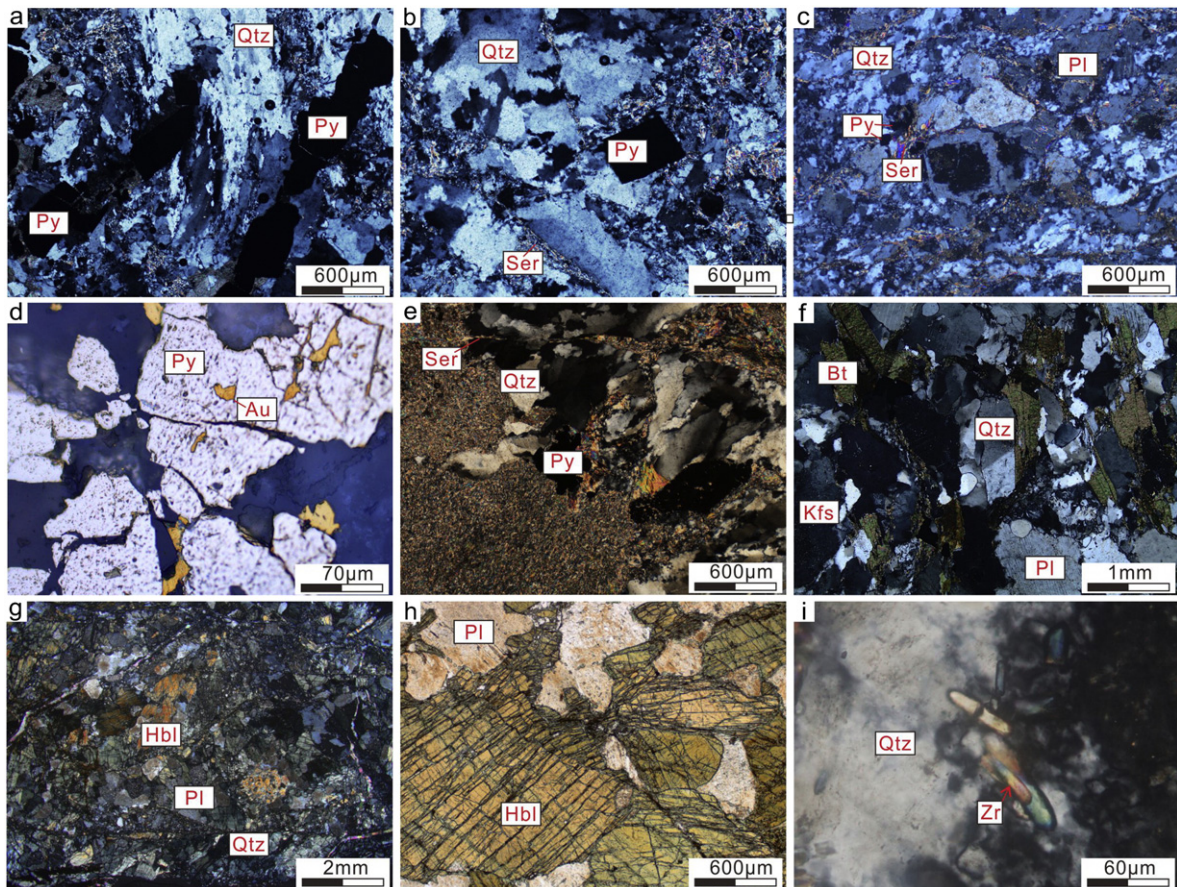


Fig. 4. Photomicrographs of microstructural features of some samples selected for zircon fission-track analyses. (a) Auriferous vein-related pyrite–sericite–quartz gold ore composed of dynamically recrystallized quartz grains associated with pyrite. (b) Dynamically recrystallized quartz grains cut by microfaults filled with sericite aggregates. (c) Disseminated- and stockwork-style ores consisting of sericite, quartz, plagioclase, and pyrite. (d) Non-refractory gold grains in microcracks within pyrite. (e) Sericite aggregates associated with pyrite cutting the dynamically recrystallized quartz vein. (f) Undeformed Linglong granite with quartz, plagioclase, K-feldspar and biotite from the footwall. (g) Amphibolite showing lepidoblastic textures, with layers of hornblende and biotite alternating with layers of quartz and plagioclase. (h) Amphibolite composed of hornblende and plagioclase. (i) Zircon grains in studied samples. Bt, biotite; Hbl, hornblende; Kfs, K-feldspar; Pl, plagioclase; Qtz, quartz; Ser, sericite; Py, pyrite; Zr, zircon. All photomicrographs in cross-polarized light except for (d).

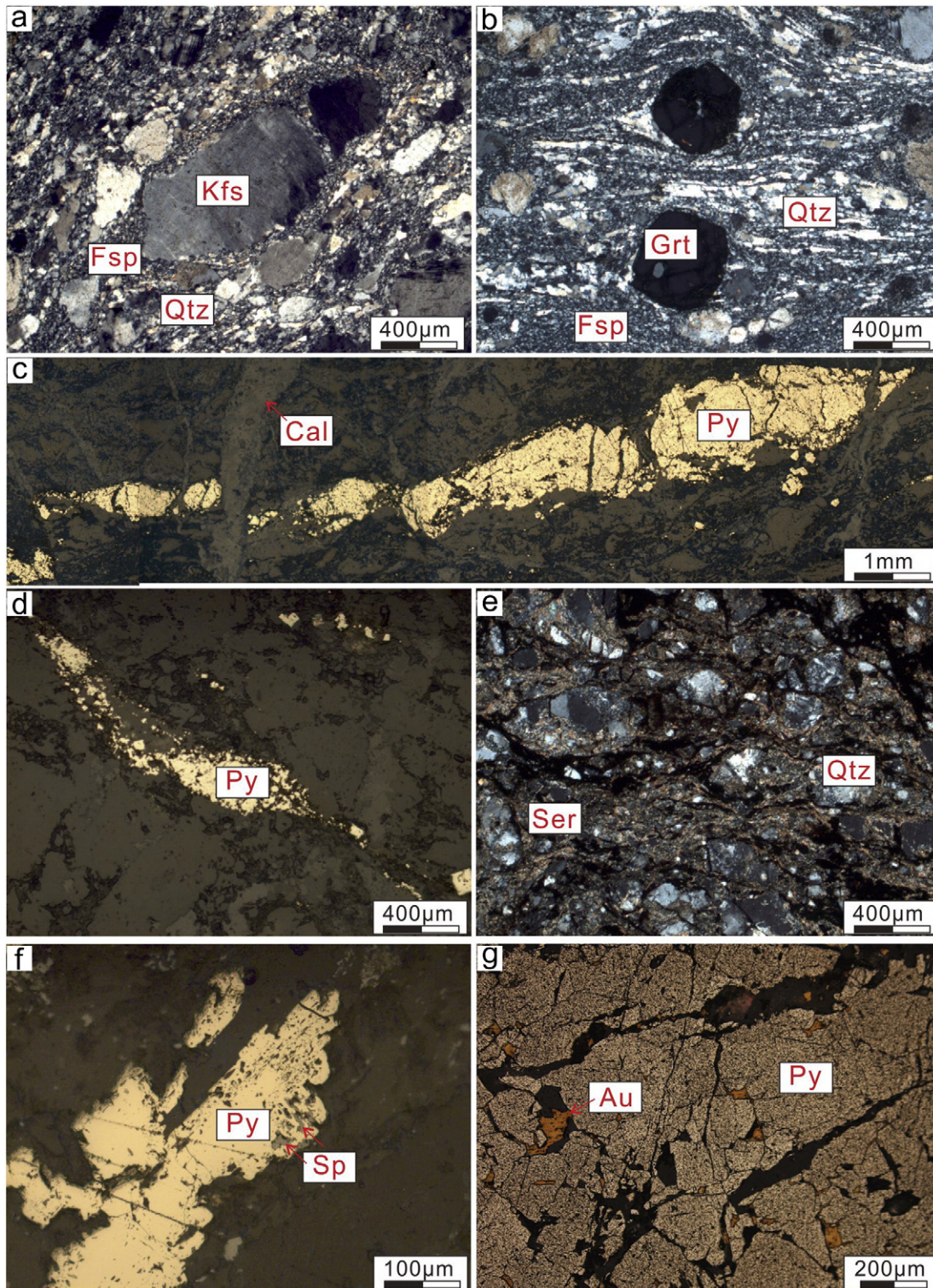


Fig. 5. Photomicrographs of deformation under cross-polarized light (a, b, e) and reflected light (c, d, f, g). (a) Photomicrograph of sigma porphyroclast of K-feldspar. (b) Photomicrograph of sigma porphyroclasts of garnet, and recrystallized quartz ribbons. (c) Pyrite aggregates forming lenses parallel to the foliation that have been stretched. (d) Foliation-parallel pyrite trails, indicating possible S–C fabric. (e) Complex breccia showing multiple events of fracturing and brecciation. (f) Zonation of pyrite with sphalerite inclusions on the outer rim. (g) Non-refractory gold grains in microcracks within pyrite. Kfs, K-feldspar; Pl, plagioclase; Fsp, feldspar; Qtz, quartz; Ser, sericite; Grt, garnet; Cal, calcite; Py, pyrite; Sp, sphalerite.

deformation. This is interpreted to indicate that the fine-grained, sericitic alteration matrix was sufficiently weak to deform ductilely even in the dominant brittle, cataclastic domain. Alternatively, brecciation may have occurred at relatively high temperature, as a result of increased pore pressure, and ductile deformation resumed after cataclasis and a drop in pore pressure.

Pyrite grains in the aggregates are fractured (Fig. 5c) and this may have occurred during the early ductile deformation or during subsequent brittle events. Sphalerite, by contrast, is late, probably post-dating ductile deformation, as it is present as inclusions in the outer rims of pyrite (Fig. 5f) and not in its cores, and also on the walls of fractures that cut early pyrite. Furthermore, despite being malleable,

sphalerite grains are not ductilely deformed. Gold is mostly in fractures in pyrite (Fig. 5g). Because pyrite deforms in a brittle fashion under most P–T conditions, fractures in pyrite could have developed at any time during alteration and deformation.

In summary, the deformation seems to be characterized by continuous hydrothermal events, starting with ductile deformation and precipitation of quartz and pyrite. This is overprinted by multiple brittle fracturing/brecciation events related to mineralization, which lead to further growth of pyrite, and overgrowth of pyrite contemporaneous with precipitation of sphalerite, and to gold precipitation in fractures in pyrite. The altered groundmass weakened the rock so that it responded ductilely even at relatively low temperatures.

3. Sampling and analytical methods

3.1. Sampling

Nine samples for ZFT analysis were collected systematically along a NW–SE transect perpendicular to the Linglong detachment fault (Fig. 3b) at the –652 m level of the Xiadian gold deposit. At this location, the footwall and hangingwall of the Linglong MCC, the detachment fault and its mylonitic to ultramylonitic rocks, the cataclastically deformed brecciated rocks and associated brittle faults and hydrothermally altered rock with the mineralization are all well exposed. In order to constrain the cooling and exhumation history of the Linglong MCC and establish the relationship between its evolution and gold genesis, rocks that underwent different degrees of deformation in the footwall and hangingwall of the detachment, as well as those in the gold ore zones, were sampled. Each sample was at least 3 kg to ensure that sufficient zircon grains could be obtained. From the footwall to the hangingwall of the detachment fault, the collected rocks were: undeformed Linglong granite (XD08) in the footwall; pyrite–sericite–quartz gold ore (XD54), pyrite–sericite–quartz altered granitic mylonite (XD46), fault gouge (XD41), pyrite–sericite–quartz altered ultramylonite (XD38), and pyrite–sericite–quartz altered breccia (XD37), all within the detachment zone; and amphibolite (XD34), fault gouge (XD32), and amphibolite (XD31) in the hangingwall (Fig. 3b).

The undeformed Linglong granite sample XD08 shows medium- to coarse-grained granular texture, and mainly contains quartz, plagioclase, K-feldspar, and biotite (Fig. 4f). The disseminated- and stockwork-style ore sample XD54 (pyrite–sericite–quartz gold ore) is composed of dynamically recrystallized quartz grains associated with gold-bearing pyrite (Fig. 4a, b), with cracks filled with sericite aggregates (Fig. 4b). Samples XD46 (pyrite–sericite–quartz altered granitic mylonite), XD38 (pyrite–sericite–quartz altered ultramylonite), and XD37 (pyrite–sericite–quartz altered breccia) consist of sericite, quartz, plagioclase, K-feldspar, pyrite (Fig. 4c), and trace amounts of chalcopyrite, galena, sphalerite, and gold. Fault gouge samples XD41 and XD32 consist mainly of illite, montmorillonite, and kaolinite (Gao, 2008). Amphibolite sample XD34 exhibits lepidoblastic textures with layers of hornblende and biotite, alternating with layers of quartz and plagioclase (Fig. 4g). Amphibolite sample XD31 is mostly composed of plagioclase and hornblende (Fig. 4h).

3.2. Analytical methods

Zircon grains were separated by conventional magnetic and heavy-liquid techniques for fission-track analyses. All the analyses were performed at the Institute of High Energy Physics of the Chinese Academy of Sciences by the external detector method (Gleadow, 1981). Zircons were embedded in polyfluoroalkoxy Teflon disc, and they were all ground and polished to expose internal grain surfaces. The zircons were etched in the KOH–NaOH eutectic mixture for 25 h at 220 °C. Irradiation of packages including the zircon mounts, as well as low-uranium muscovite external detectors, and CN2 uranium dosimeter glasses that were used as a neutron fluence monitor for each sample (Yuan et al., 2009), was carried out in the 492 Swim-Pool hot-neutron nuclear

reactor. The reactor is well thermalized with a cadmium ratio of >100 for Au, at the China Institution of Atomic Energy, Beijing. Following irradiation, low-uranium muscovite, used as an external detector, was etched in 40% HF for 20 min at 25 °C to reveal the induced fission tracks. The track densities in both natural (ρ_n) zircon grains without fluid inclusions and fractures (Fig. 4i), and induced (ρ_i) fission-track populations in the muscovite external detectors, as well as the induced track densities of dosimeter glasses (ρ_d), were measured at 1000× magnification on screen photos.

Where possible, >20 crystals of each sample were counted for age determination. The central ages for the populations (Galbraith and Laslett, 1993) were calibrated by the Zeta calibration method (Hurford and Green, 1983), with a zeta value of 85.4 ± 4 , and 1σ errors were calculated using the techniques of Galbraith (1981, 1984). The Chi-square (χ^2) test was employed to determine if the analyzed grains belong to a single population of ages (Galbraith, 1981). The amount of uranium present was calculated based on the track densities, known proportion of isotopes of uranium, and the uranium content of the dosimeter glasses.

Fission tracks generated in the partial annealing zone (Wagner and Haute, 1992) continued to fade until the temperature was too low to reduce track densities (Guedes et al., 2013). This resulted in the apparent age corresponding to the time when there was no additional density reduction, rather than to the actual beginning of the generation of the fission tracks. In other words, ZFT ages constrained the time that zircon grains cooled through their effective closure temperature (Dodson, 1973). The resulting ZFT ages were interpreted to represent the cooling age of the zircon through the temperature of $\sim 240 \pm 50$ °C (Bernet, 2009; Hurford, 1986; Zaun and Wagner, 1985) suggested by field-based estimations, which is a lower range than the 200–360 °C (Brandon et al., 1998; Yamada et al., 1995) given by annealing models.

4. Results and interpretation

Nine samples, collected from the three units of Linglong MCC (the footwall, the hangingwall, and the detachment fault zone), yielded nine ZFT central ages (Table 1). Representative single-grain age distributions of these samples are shown in Fig. 6 using radial plots (Galbraith and Laslett, 1993) created by RadialPlotter software (Vermeesch, 2009). These central ages vary from 136.9 ± 3.3 Ma (1σ) to 114.9 ± 8.7 Ma (1σ). The χ^2 test shows that five samples have $P(\chi^2)$ of 0%, while the other four samples range from 6% to 39% (Table 1). Typically, the low $P(\chi^2)$ values are considered to contain ≥ 2 grain age components (O'Sullivan and Parrish, 1995; Brandon, 2002). Because the protolith along the detachment zone is the very same Linglong granite (Fig. 3), the low $P(\chi^2)$ should not have been caused by zircon grains from different sources. Different annealing properties of different grains are related to differences in radiation damage and mainly reflect variations in uranium content between grains in the same sample (Tagami et al., 1990; Marsellos and Garver, 2010; B. Kohn, 2015, personal communication). However, these grains lack systematic changes with uranium content (Fig. 6), whereas their uranium contents are typically low, varying in a narrow range between 95 and 196 ppm (Fig. 6). Given that the Linglong granite with low-uranium zircon grains is relatively young (163–155 Ma), little radiation damage is expected (Marsellos and Garver, 2010). We argue, therefore, that it is unlikely the low $P(\chi^2)$ values are due to radiation damage or multiple age groups.

It is most likely that the wide spread in ages leading to the low $P(\chi^2)$ of some samples relates to introduced errors. In the radial plots, the single grain ages are relatively concentrated, except for a few points outside the main range. It is these few grains that lead to the failure of the χ^2 test, which cannot cause any obvious influence on the central ages (Galbraith, 1984). Therefore, we interpret the central ages as most representative of the ZFT ages of the samples and use them in this study. For hangingwall samples XD31 and XD32, with low $P(\chi^2)$

Table 1
Zircon fission-track data measured on the samples from the Xiadian gold deposit. Note: ρ_d is induced track density measured on dosimeter glasses, ρ_i is induced track densities measured on mica external detectors, ρ_s is the spontaneous track density on internal mineral surface. N_d and N_i are the number of tracks on dosimeter glasses and external detectors, and N_s is the number of tracks on mineral surfaces. $P(\chi^2)$ is the chi-square probability (Galbraith, 1981); values lower than 5% are considered to fail this test. LDF, Linglong detachment fault.

Sample no.	Location	Rock type	Number of grains	ρ_d (N_d) ($\times 10^5 \text{ cm}^{-2}$)	ρ_s (N_s) ($\times 10^5 \text{ cm}^{-2}$)	ρ_i (N_i) ($\times 10^5 \text{ cm}^{-2}$)	U (ppm)	$P(\chi^2)$ (%)	Central age $\pm 1\sigma$ (Ma)	Recalculated $P(\chi^2)$ (%)	Recalculated central age $\pm 1\sigma$ (Ma)
XD08	Footwall	Undeformed biotite granite	24	30.617 (31,085)	144.913 (6339)	138.352 (6052)	162.7	6	135.0 \pm 3.0	/	/
XD54	The LDF	Pyrite-sericite-quartz gold ore	25	30.874 (31,085)	128.556 (7102)	128.990 (7126)	149.4	39	130.1 \pm 2.2	/	/
XD46	The LDF	Pyrite-sericite-quartz granitic mylonite	24	31.194 (31,085)	146.275 (7060)	146.689 (7080)	172.1	0	130.5 \pm 3.4	/	/
XD41	The LDF	Fault gouge	3	31.451 (31,085)	92.339 (472)	107.012 (547)	122.5	14	114.9 \pm 8.7	/	/
XD38	The LDF	Pyrite-sericite-quartz ultramylonite	24	31.707 (31,085)	120.942 (5124)	122.854 (5205)	142.1	0	130.8 \pm 3.6	/	/
XD37	The LDF	Pyrite-sericite-quartz breccia	24	31.963 (31,085)	105.233 (4986)	109.623 (5194)	123.0	0	130.7 \pm 3.8	/	/
XD34	Hangingwall	Weakly deformed amphibolite	24	32.220 (31,085)	147.803 (6262)	148.605 (6296)	171.0	8	135.0 \pm 2.9	/	135.5 \pm 4.9
XD32	Hangingwall	Fault gouge	24	32.733 (31,085)	145.103 (3409)	140.080 (3291)	156.2	0	141.4 \pm 6.2	1	136.9 \pm 3.3
XD31	Hangingwall	Unstrained amphibolite	24	32.476 (31,085)	106.691 (5978)	98.428 (5515)	164.6	0	143.8 \pm 5.0	14	/

values of zero, a few zircon grains yielded anomalously higher ages and cause a dispersal in the age pattern, which is indicated by the failure to pass the Chi-square test. We removed the zircon grains that cluster at these high ages (top right corner of diagram) and recalculated the central age without them. Less dispersion is obvious and we obtain a central age of 136.9 ± 3.3 Ma (1σ) and 135.5 ± 5.5 Ma (1σ), respectively, for the two hangingwall samples. The single-grain ages that were removed might indicate that there was a more complex cooling history of the amphibolite, although given the very few grains, this is far from certain. Detailed ZFT results are summarized below.

4.1. The footwall and hangingwall

Sample XD08, from the undeformed footwall Linglong granite, located ~1 km to the west of the Linglong detachment fault, yielded a ZFT central age of 135.0 ± 3.0 Ma (1σ) (Table 1).

Samples XD34 and XD31, from the fresh amphibolite in the hangingwall, have zircon central ages of 135.0 ± 2.9 Ma (1σ) and 136.9 ± 3.3 Ma (1σ) (Table 1), which is younger than the 160 Ma emplacement age of Linglong granite in the footwall, but identical to its ZFT footwall cooling age (sample XD08).

Sample XD32 was collected from a 1–3 cm-wide gouge zone on the NE-trending brittle fault in the amphibolite. It yielded a ZFT central age of 135.5 ± 4.9 Ma (1σ) (Table 1), which is similar to that of its host rock (sample XD31) suggesting that late, low-temperature faulting did not reset the ZFT age.

4.2. Linglong detachment zone

Sample XD54 from the pyrite-sericite-quartz altered disseminated ore zone adjacent to an auriferous quartz vein, yielded a zircon central age of 130.1 ± 2.2 Ma (1σ) (Table 1), younger but within error of the unaltered footwall and hangingwall samples. Folded pyrite aggregates and recrystallized quartz associated with gold-bearing pyrite (Fig. 4a, b) deposited during ductile deformation suggest that mineralization may have started at temperatures as high as 300–350 °C, which are slightly higher than the closure temperature of the ZFT method. Therefore, this could reflect a ZFT age that has cooled from an early hydrothermal stage to a slightly lower closure temperature of 240 ± 50 °C. Thus, the three samples taken in the stockwork-disseminated ores along the detachment fault, described below, might more convincingly reflect the mineralization age because the temperature of the gold event was likely similar to, or just slightly above, the ZFT closure temperature.

Three samples from the disseminated- and stockwork-style ores, XD46, XD38 and XD37 (Table 1), have similar ZFT central ages of 130.5 ± 3.4 Ma (1σ), 130.8 ± 3.6 Ma (1σ), and 130.7 ± 3.8 Ma (1σ) (Table 1). These ages are similar to that of sample XD54, and also represent magmatic zircons that have been reset by the hydrothermal alteration, but at a temperature lower than that which was responsible for the resetting of sample XD54.

Sample XD41, which was collected from a 2–5 cm-wide gouge zone in the NE-trending brittle fault in pyrite-sericite-quartz altered ultramylonite, yielded a zircon central age of 114.9 ± 8.7 Ma (1σ) (Table 1). Because this is based on only three zircon grains, the significance of this age is not clear and will not be considered further.

In summary, the ZFT ages for the three rock groups (unaltered wallrocks including Mesozoic granite and Late Archean basement rock, hydrothermally-altered wallrocks, and fault gouge) in this study vary from 136.9 ± 3.3 Ma (1σ) Ma to 130.1 ± 2.2 (1σ). The unaltered Linglong granite in the footwall of the Linglong detachment fault and the two unaltered amphibolite samples in the hangingwall of the Linglong detachment fault provide similar cooling ages for the MCC. The fission-track data suggest the entire MCC cooled below about 240 ± 50 °C at ca. 137–135 Ma. Reset ZFT central ages from the disseminated- and stockwork-style ores indicate cooling of the mineralization below 240 ± 50 °C at ca. 131–130 Ma (samples XD54,

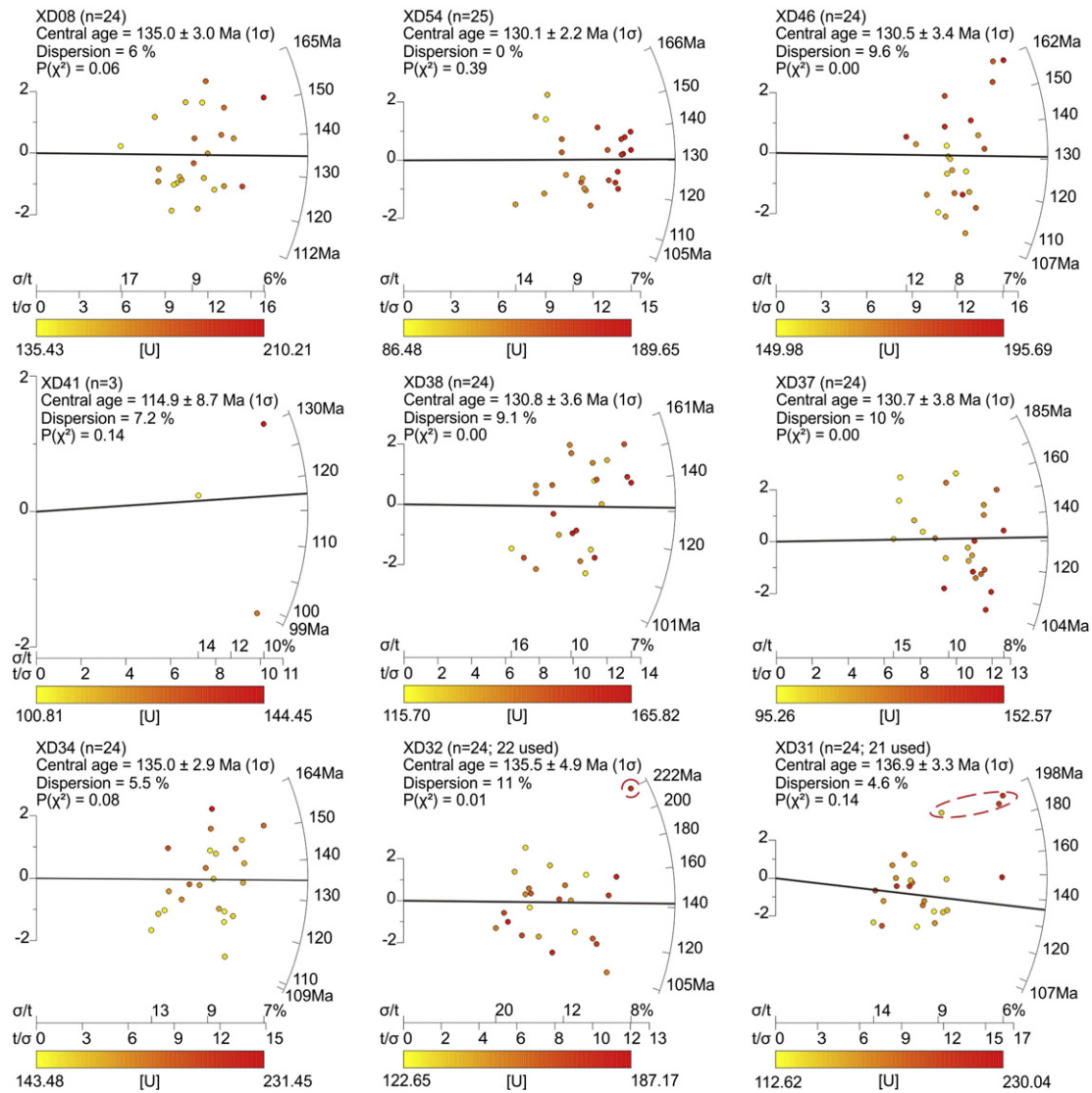


Fig. 6. Radial plots of zircon samples. Single-grain ages are read off the intersection between a line linking the origin with the single grain point and the arc. The σ/t and t/σ on X-axis indicate the relative error and precision, respectively, of each single-grain age, and the Y-axis depicts the standard error of each measurement. Continuous thick lines represent the central ZFT ages listed in Table 1. Color of single-grain ages are coded and linked to the color bar at the bottom of each plot and represent the uranium content of single zircon grains. Single-grain ages circled by the dashed line (top right corner of the plot) for samples XD31 and XD32 have not been used to calculate the central ages.

XD46, XD38, and XD37). Whereas the one-sigma error bars still suggest that overlap is possible, the two distinct groups of determined ages provide fairly convincing evidence that the gold event took place about 5 million years subsequent to cooling of the MCC below the ZFT closure temperatures.

5. Discussion

5.1. Evolution of the Linglong Metamorphic Core Complex

The ZFT ages and their effective closure temperatures of 240 ± 50 °C are plotted in Fig. 7 to assess the cooling histories. The time-temperature evolution of the Linglong MCC is further constrained by the zircon U–Pb ages of 163–155 Ma (Ma et al., 2013; Yang et al., 2012) and the magmatic muscovite $^{40}\text{Ar}/^{39}\text{Ar}$ age of 143 ± 1.5 Ma (Charles et al., 2013) for the Linglong granite (Figs. 2a and 7), and an amphibole $^{40}\text{Ar}/^{39}\text{Ar}$ age of 207 ± 4 Ma (Faure et al., 2003) for the amphibolite in the hangingwall (Figs. 2a, 7). We assume the minimum crystallization temperature for magmatic zircon

to be ~ 700 °C (Watson and Harrison, 2006), and the $^{40}\text{Ar}/^{39}\text{Ar}$ closure temperatures for amphibole and muscovite to be 575 ± 25 °C (Daoudene et al., 2013) and 400 ± 50 °C (Hames and Bowring, 1994; McDougall and Harrison, 1999), respectively, at a relatively rapid cooling rate. In the following discussion, only average cooling rates based on the central ages, without the addition and subtraction errors, are calculated. Monotonic and relatively rapid cooling is required for thermochronological data in calculating cooling rates through the closure-temperature model (Braun et al., 2006). Due to the wide range of closure temperatures and errors of cooling ages, the uncertainties of the cooling rates are high (Spotila, 2005; Braun et al., 2006).

Combined with the amphibole $^{40}\text{Ar}/^{39}\text{Ar}$ age of 207 ± 4 Ma for the amphibolite from the northeastern part of the Linglong MCC, the ZFT ages of 136.9 ± 3.3 Ma and 135.0 ± 2.9 Ma obtained in this study for the hangingwall amphibolites indicate cooling from ~ 575 °C to ~ 240 °C at an average rate of 5 °C/m.y.. However, rare zircon grains with older ages for samples XD31 and XD32 might indicate a more complex cooling history.

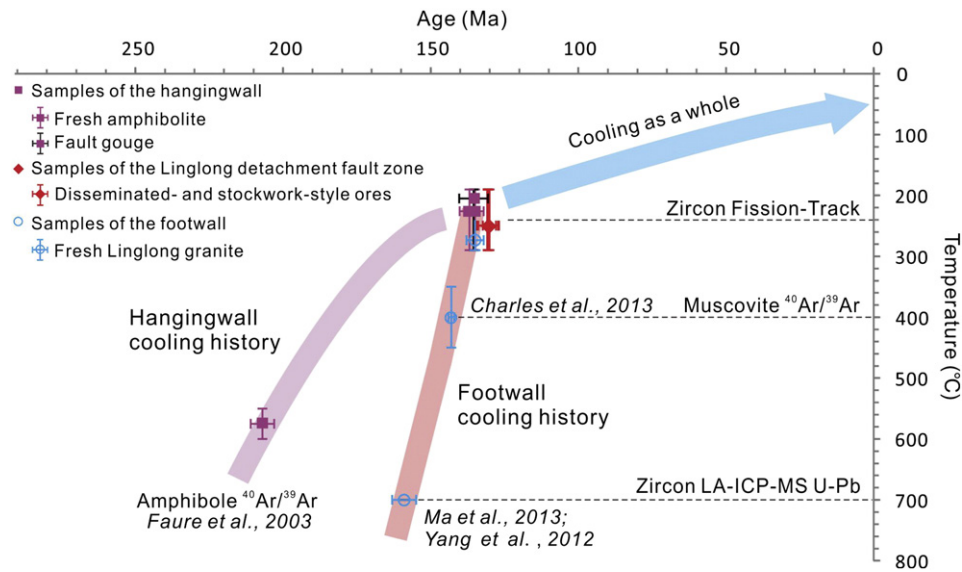


Fig. 7. Temperature–time evolution of the Linglong Metamorphic Core Complex drawn on the basis of U–Pb, $^{40}\text{Ar}/^{39}\text{Ar}$, and fission-track ages. Ages other than fission-track ages are for zircon U–Pb ages of 163–155 Ma (Ma et al., 2013; Yang et al., 2012), an amphibole $^{40}\text{Ar}/^{39}\text{Ar}$ age of 207 ± 4 Ma (Faure et al., 2003), and a magmatic muscovite $^{40}\text{Ar}/^{39}\text{Ar}$ age of 143 ± 1.5 Ma (Charles et al., 2013).

Using the LA-ICP-MS zircon U–Pb age of ca. 163–155 Ma for crystallization of the Linglong granite (Figs. 2a, 7), and its $^{40}\text{Ar}/^{39}\text{Ar}$ muscovite age of 143 ± 1.5 Ma, from a sample ~25 km to the west of the Linglong detachment fault (Fig. 2), we infer that the footwall cooled to 400 °C at an average rate of ~19 °C/m.y. after granite emplacement (Fig. 7). The next granite cooling step from about 400 °C to 240 °C has large uncertainties because of the large errors on the ZFT ages, which hinder precise constraints. Using the central ZFT age of the 135.0 ± 3.0 Ma range determined for the granite (Fig. 7), we estimate an average cooling rate of 20 °C/m.y., broadly in line with the preceding history.

The ZFT ages of 135.0 ± 2.9 Ma and 136.9 ± 3.3 Ma of fresh amphibolite samples from the hangingwall overlap within error that of the footwall granite at 135.0 ± 3.0 Ma (Fig. 8), and the ZFT ages of ore samples are between 134.5 and 126.9 Ma at one-sigma uncertainty and thus within error of the cooling ages of the surroundings. We infer that mineralization occurred against a background of temperatures close to the ZFT closure temperatures, where hydrothermal fluids were mainly in the range of 240–300 °C, as shown by the fluid-inclusion studies. Mineralization is also contemporaneous with the crystallization of the 132–123 Ma Guojialing granitoids, which were presumably part of the same tectonothermal extensional event, although they show no obvious spatial association with the gold deposits.

The fault gouge most likely developed at temperatures below 240 °C given its clay mineralogy, and its ZFT age of 114.9 ± 8.7 Ma (sample

XD41); this age was based on only three zircons and is therefore not discussed in detail. However, the presence of the fault gouge cutting the ca. 130 Ma mineralization suggests significant normal movement on this detachment that may have induced different levels of denudation, but this has not resulted in significantly different cooling ages between the hangingwall and footwall. We find that there are four possible reasons for this: (a) all significant fault movement occurred at temperatures above the 240 ± 50 °C ZFT closure temperature after which the hangingwall and footwall cooled as a single block; (b) movement was sufficiently slow so as not to shift significantly the position of the isotherms across the fault; (c) displacement of the isotherms were significant, but the uncertainties in the cooling ages are too large and mask any cooling time differences; and (d) our hangingwall samples were too close to the fault and were rapidly equilibrated with the footwall temperatures. Option (a) is unlikely because the presence of a well-developed fault gouge overprinting ductile mylonites suggests late faulting in a relatively cold environment, at temperatures between the annealing temperatures of zircon and apatite (Zwingmann and Mancktelow, 2004). Options (b) and (c) are two aspects of the same problem. The displacement of the isotherms resulted from a balance between the movement rate on the fault causing upward displacement of the isotherms in the footwall, and denudation of the uplifted block that would cool the block. At relatively shallow crustal levels, where we expect the fault gouge to have developed, the geothermal gradient imposed by

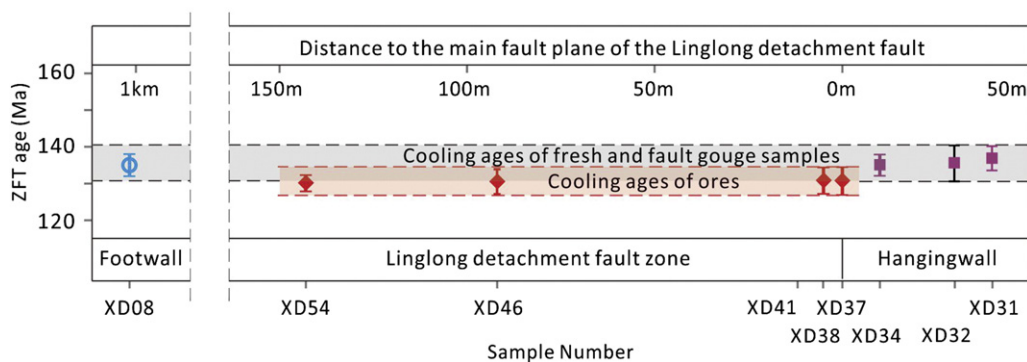


Fig. 8. Low-temperature thermochronometric age–distance plots showing zircon fission-track ages with 1 σ error bars, respectively, for samples projected at right angles onto profile A–A' in Fig. 3. LDF, Linglong detachment fault. Legend as in Fig. 7.

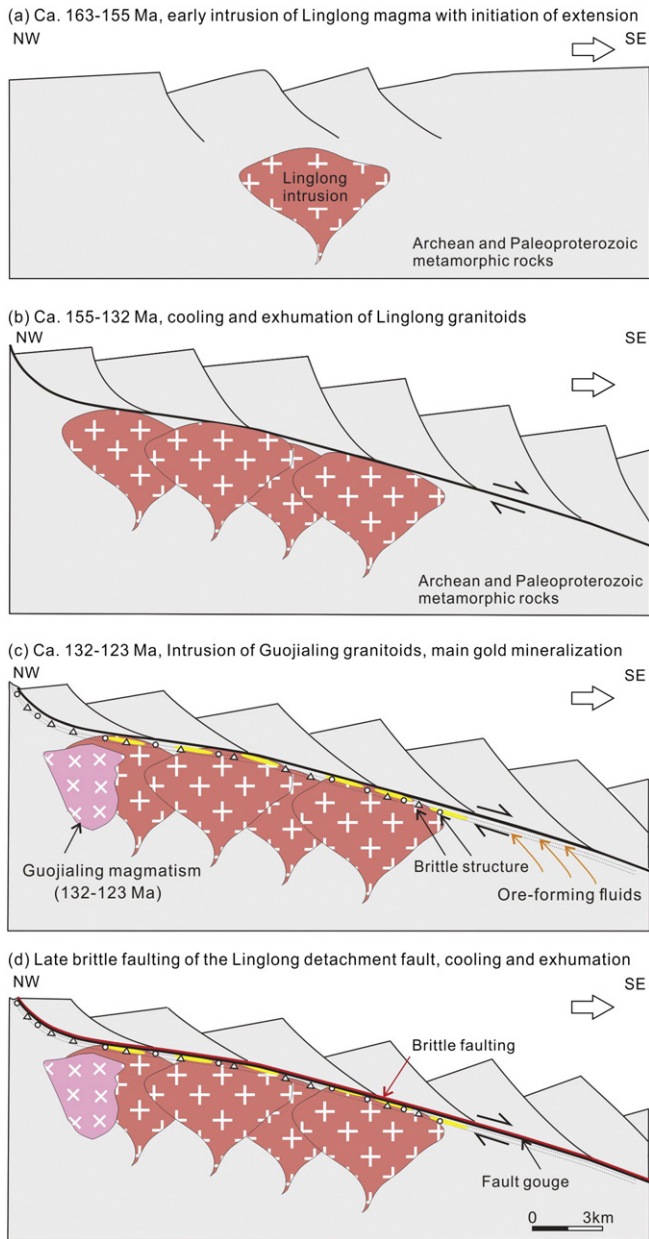


Fig. 9. Cooling and exhumation histories of the Linglong Metamorphic Core Complex. (a) Early intrusion of Linglong magma associated with initiation of regional extension (163–155 Ma; Charles et al., 2013; Ma et al., 2013; Yang et al., 2012); (b) Cooling and exhumation of Linglong granitoids (155–132 Ma; Charles et al., 2013). (c) Intrusion of Guojialing granitoids (132–123 Ma; Yang et al., 2012; Liu et al., 2014a, b; Wang et al., 2014); hot hydrothermal fluids (main phase of gold mineralization) at ca. 131–130 Ma; (d) Brittle faulting of Linglong detachment, late cooling, and exhumation.

the fixed temperature at the cool surface of the Earth restricts relatively fast cooling. Compounding the problem, the large uncertainties associated with the cooling ages, between 5 and 10 m.y. at the two sigma level or 7% of the ZFT ages, may mask differences in cooling time. The combination of fast cooling (options (b and c)), large uncertainties (option (c)), and the proximity of the hangingwall sample to the fault (option (d)), could together explain the apparent age coincidence between cooling ages of the hangingwall and footwall samples.

Based on the above, the evolution of the Linglong MCC can be constrained (Figs. 7, 9). The hangingwall of the MCC cooled to below about 240 °C at 136 Ma (Fig. 7), more than 20 m.y. after intrusion and crystallization of the Linglong granitoid host (163–155 Ma; Yang et al., 2012), which correlates with the initiation of regional extension (Charles et al., 2013; Fig. 9a). The Linglong granitoids cooled to about

400 °C by 143 Ma at the rate of about 19 °C/m.y. (Fig. 9b) and continued to cool at approximately the same rate to 240 ± 50 °C by 135.0 ± 3.0 Ma, during exhumation along the Linglong detachment fault. Hydrothermal fluid flow along the fault, responsible for gold deposition and the alteration, reset the zircons at about 131–130 Ma, which was also contemporaneous with intrusion of the Guojialing granitoids (Fig. 9c). At this time, we envisage a relatively cool country-rock environment temperature of about 240 °C, although granitoid intrusion would have imposed a local steep horizontal geothermal gradient. Faulting continued as the thermal event ended, giving rise to the fault gouge that cuts the mineralization (Fig. 9d).

5.2. Timing of ore-forming hydrothermal activity in the Xiadian and adjacent gold deposits

Abundant age constraints of variable quality have been published for the gold deposits in the Linglong MCC (Yang et al., 2007a; Guo et al., 2013), suggesting that hydrothermal alteration took place at ca. 120 ± 10 Ma (Yang et al., 2007b). In detail, the large gold deposits located adjacent to the Jiaojia fault zone, on the western margin of Linglong MCC, formed between 125 and 115 Ma (Li et al., 2003; Zhang et al., 2003). For example, the sericite $^{40}\text{Ar}/^{39}\text{Ar}$ plateau ages for the Jiaojia, Xincheng, and Wang'ershan deposits yield a consistent age centered around 120 Ma with very small errors of 0.6 m.y., 0.3 m.y., and 0.2 m.y., respectively (Li et al., 2003). Along the eastern margin of the Linglong MCC, there are few age data. However, recent $^{40}\text{Ar}/^{39}\text{Ar}$ sericite and muscovite dating of the Dayingezhuang gold deposit, 15 km north of the Xiadian deposit (Fig. 2) suggest that the main phase of gold mineralization there was also 130 ± 4 Ma (Yang et al., 2014c). This further supports our suggestion that resetting of country-rock zircons during a hydrothermal gold event can result in fission-track dating methods being useful in providing a meaningful approximation of the age of the event.

Sample XD54 from the mineralized detachment fault zone yielded a ZFT age of 130.1 ± 2.2 Ma (Table 1; Fig. 6). This sample has evidence of ductile deformation in the form of recrystallized quartz grains associated with gold-bearing pyrite (Fig. 4a, b). This suggests that initial hydrothermal temperatures were maintained at 300–350 °C long enough for ductile strain to accumulate. The other three ore-zone samples yielded similar ZFT ages of 130.5 ± 3.4 Ma, 130.8 ± 3.6 Ma, and 130.7 ± 3.8 Ma. Given that the surrounding country rocks were already close to or below ZFT closure temperature by ca. 135 Ma, these consistent ages suggest a 131–130 Ma ore-forming event. Brittle deformation and associated hydrothermal activity (Fig. 5) were probably part of the same overall event.

5.3. Structural control of the Linglong Metamorphic Core Complex on gold mineralization

Microstructures show that the deformation started with ductile events and deposition of pyrite (Fig. 5), and the ductile features were overprinted by multiple brittle fracturing/brecciation events and hydrothermal alteration leading to further growth of pyrite, and precipitation of sphalerite and gold. Ductile deformation of altered rocks may have taken place at relatively low temperatures due to the considerable modal proportions of fine-grained sericite, giving rise to a weak rock. Therefore, we suggest that the Xiadian deposit is a product of a major gold-forming hydrothermal event occurring near the brittle–ductile transition along the detachment between the metamorphic rocks of the hangingwall and Mesozoic intrusions of the footwall (Fig. 9c).

The Jiaodong Peninsula is one of the largest known granitoid-hosted gold provinces in the world (Li et al., 2012) and its gold deposits are unlike those of Archean cratons, such as those in Canada and Western Australia. In Jiaodong, gold deposits are hosted dominantly by late Mesozoic granitoids, which formed at least 2 b.y. after metamorphism

of the Archean Jiaodong basement rocks (Chen et al., 2004; Fan et al., 2005; Goldfarb et al., 2007; Wang et al., 2015).

It is widely accepted that during the Early Cretaceous, eastern Asia experienced NW–SE extensional tectonism, as supported by data from the many MCCs (Yagan–Onch Hayrhan, Yiwulüshan, South Liaonan, Gudaoling) across the North China Craton and the widespread 130–110 Ma magmatism (Davis et al., 1996; Lin et al., 2008; Yang et al., 2012; Wang et al., 2014; Boorder, 2015; Yang and Santosh, 2015; Fig. 1). Recent studies show that 156–138 Ma ages represent the initial formation of the Erendavaa MCC in Mongolia (Daoudene et al., 2013), and that Late Jurassic to Early Cretaceous extensional tectonics occurred in the South Liaodong Peninsula as supported by the development of the South Liaonan MCC (Lin et al., 2008). Furthermore, Late Jurassic sediments, which fill the Songliao Basin, suggest a Late Jurassic extensional setting for this area (Lin et al., 2003). In the Jiaodong Peninsula, the Linglong MCC developed contemporaneously with intrusion of the synkinematic 132–123 Ma Guojialing granitic suite that was followed by the post-tectonic 118–110 Ma Aishan granitic suite. Thus, MCC development, large-scale magmatism, and gold mineralization took place contemporaneously during the Early Cretaceous.

Thermomechanical convective removal of lithosphere, post-orogenic collapse, and mantle plume events, have all been invoked to explain a continental extensional tectonic event (Meng, 2003; Lin and Wang, 2006; Zhao et al., 2007). However, all of the models above are difficult to apply in explaining such a long extensional period that lasted for at least ~60 m.y. (Corti et al., 2003; Charles et al., 2011a, 2013). The long duration of extensional tectonics in eastern Asia is likely explained by the progressive slab rollback of the paleo-Pacific plate from 160 Ma onward (Maruyama et al., 1997; Charles et al., 2013). We suggest therefore that the Early Cretaceous gold mineralization in Jiaodong occurred in an extensional regime caused by the progressive slab rollback of the paleo-Pacific plate.

The MCCs along the margins of the North China Craton control much of the gold mineralization (Fig. 1). For example, several MCCs (Sun et al., 2013) control many gold deposits within the southern margin of the craton (Fig. 1b), the second largest gold producing area in China. The Yiwulüshan (Zhu et al., 2002) and Liaonan MCCs (Liu et al., 2005) also control numerous gold deposits (Fig. 1) within the northern border of the craton. These gold orebodies formed during movement on the detachment faults. For instance, the Queshan MCC and its detachment system controlled the formation of the Guocheng and Pengjiakuang gold deposits at ca. 120 Ma (Yang et al., 2000; Shen et al., 2002; Zhang et al., 2003). Such temporal and spatial coincidences imply that the MCCs have apparently controlled the gold mineralization. Large gold orebodies are typically concentrated within 100 m of the footwall of the detachment faults, where late brittle deformation and large-scale alteration overprint the early brittle–ductile transition zone, both in the Linglong MCC and in other similar environments in the eastern North China Craton.

6. Conclusions

Fission-track data from the Xiadian gold deposit constrain the cooling history of the Linglong MCC and the timing of mineralization. The Linglong granite in the footwall of the Linglong detachment fault was emplaced at ca. 163–155 Ma, cooled to about 400 °C by 143 Ma, and then to 240 °C by 135.0 ± 3.0 Ma (1 σ), presumably as a result of exhumation along the detachment fault. Mineralization took place at temperatures close to ZFT closure and therefore ZFT ages provide an approximate age for mineralization. Four samples from the altered granite of the Xiadian deposit yielded consistent ZFT ages centered at ca. 131–130 Ma and likely mark the main gold event. This age is similar to that estimated for the Dayingezhuang gold deposit also on the east margin of the Linglong MCC, but is unlike that for deposits on the western margin of the complex, which formed at ~120 Ma, suggesting a temporal evolution of the mineralization from east to west.

Movement of the Linglong detachment fault continued after the end of mineralization process as evidenced by the presence of low-temperature fault gouge truncating the mineralization, separating the Archean–Paleoproterozoic metamorphic rocks from the orebodies and the Mesozoic intrusions. The mineralization and cooling occurred in an extensional regime that may have resulted from the progressive slab rollback of the paleo-Pacific plate.

Conflict of interest

No conflict of interest exists in the submission of this manuscript, and manuscript is approved by all authors for publication. I would like to declare on behalf of my co-authors that the work described was an original research that has not been published previously, and not under consideration for publication elsewhere, in whole or in part. All the authors listed have approved the manuscript that is enclosed.

Acknowledgements

Insightful and thorough reviews by three anonymous referees and excellent comments and support from Professor Barry Kohn and Doctor Guangwei Li at Melbourne University have helped us improve the paper significantly. We thank Tony Cockbain for his assistance with editing of the text. This work was financially supported by the National Natural Science Foundation of China (Grant No. 41230311), the National Science and Technology Support Program of China (Grant No. 2011BAB04B09), the geological investigation work project of China Geological Survey (Grant No. 12120114034901), the 111 Project (Grant No. B07011) and the CSC Scholarship Program of China (File Nos. 201406400008 and 201506400079).

References

- Bernet, M., 2009. A field-based estimate of the zircon fission-track closure temperature. *Chem. Geol.* 259 (3), 181–189.
- Boorder, H.D., 2015. The Jiaodong gold district, northeastern China, in the context of the Late Paleozoic and Late Mesozoic large igneous provinces, orogeny and metallogeny in Eurasia. *Ore Geol. Rev.* 65, 574–588.
- Brandon, M.T., 2002. Decomposition of mixed grain age distributions using binomfit. *On Track* 24, 13–18.
- Brandon, M.T., Mary, K., Roden-Tice, J.I., 1998. Garver, Late Cenozoic exhumation of the Cascadia accretionary wedge in the Olympic Mountains, northwest Washington State. *Geol. Soc. Am. Bull.* 110 (8), 985–1009.
- Braun, J., Peter, V.D.B., Geoffrey, B., 2006. *Quantitative Thermochronology: Numerical Methods for the Interpretation of Thermochronological Data*. Cambridge University Press, London.
- Charles, N., Chen, Y., Augier, R., Gumiaux, C., Lin, W., Faure, M., Monié, P., Choulet, F., Wu, F.Y., Zhu, R.X., Wang, Q., 2011a. Palaeomagnetic constraints from granodioritic plutons (Jiaodong Peninsula): new insights on Late Mesozoic continental extension in eastern Asia. *Phys. Earth Planet. Inter.* 187, 276–291.
- Charles, N., Gumiaux, C., Augier, R., Chen, Y., Zhu, R.X., Lin, W., 2011b. Metamorphic core complexes vs. synkinematic plutons in continental extension setting: insights from key structures (Shandong Province, eastern China). *J. Asian Earth Sci.* 40, 261–278.
- Charles, N., Gumiaux, C., Augier, R., Chen, Y., Faure, M., Lin, W., Zhu, R.X., 2012. Metamorphic core complex dynamics and structural development: field evidences from the Liaodong Peninsula (China, East Asia). *Tectonophysics* 560, 22–50.
- Charles, N., Augier, R., Gumiaux, C., Monié, P., Chen, Y., Faure, M., Zhu, R.X., 2013. Timing, duration and role of magmatism in wide rift systems: insights from the Jiaodong Peninsula (China, East Asia). *Gondwana Res.* 24, 412–428.
- Chen, Y.J., Pirajno, F., Lai, Y., Li, C., 2004. Metallogenic time and tectonic setting of the Jiaodong gold province, eastern China. *Acta Petrol. Sin.* 4, 907–922 (in Chinese with English abstract).
- Corti, G., Bonini, M., Conticelli, S., Innocenti, F., Manetti, P., Sokoutis, D., 2003. Analogue modelling of continental extension: a review focused on the relations between the patterns of deformation and the presence of magma. *Earth Sci. Rev.* 63, 169–247.
- Daoudene, Y., Gapais, D., Ledru, P., Cocherie, A., Hocquet, S., Donskaya, T.V., 2009. The Erendavaa Range (north-eastern Mongolia): an additional argument for Mesozoic extension throughout eastern Asia. *Int. J. Earth Sci.* 98, 1381–1393.
- Daoudene, Y., Ruffet, G., Cocherie, A., Ledru, P., Gapais, D., 2013. Timing of exhumation of the Erendavaa Metamorphic Core Complex (north-eastern Mongolia) – U–Pb and ⁴⁰Ar/³⁹Ar constraints. *J. Asian Earth Sci.* 62, 98–116.
- Davis, G.A., Qian, X.L., Zheng, Y.D., Yu, H., Wang, C., Tong, H.M., Gehrels, C.E., Shafiqullah, M., Fryxell, J.E., 1996. Mesozoic deformation and plutonism in the Yunmeng Shan: a Chinese metamorphic core complex north of Beijing, China. In: Yin, A., Harrison, T.M. (Eds.), *The Tectonic Evolution of Asia*. Cambridge University Press, Cambridge, pp. 253–280.

- Davis, G.A., Darby, B.J., Zheng, Y., Spell, T.L., 2002. Geometric and temporal evolution of an extensional detachment fault, Hohhot metamorphic core complex, Inner Mongolia, China. *Geology* 30 (11), 1003–1006.
- Deng, J., Zhai, Y.S., Wang, J.P., Yang, L.Q., Fan, Y., Sun, Z.S., 2000. Shear alteration, mass transfer and gold mineralization: an example from Jiaodong ore deposit concentrating area, Shandong, China. *J. China Univ. Geosci.* 11, 281–287.
- Deng, J., Liu, W., Sun, Z.S., Wang, J.P., Wang, Q.F., Zhang, Q.X., Wei, Y.G., 2003a. Evidence of mantle-rooted fluids and multi-level circulation of ore-forming dynamics: a case study from the Xiadian gold deposit, Shandong Province, China. *Sci. China Ser. D* 46, 138–142.
- Deng, J., Yang, L.Q., Sun, Z.S., Wang, J.P., Wang, Q.F., Xin, H.B., Li, X.J., 2003b. A metallogenic model of gold deposits of the Jiaodong granite–greenstone belt. *Acta Geol. Sin.* 77, 537–546.
- Deng, J., Yang, L.Q., Ge, L.S., Wang, Q.F., Zhang, J., Gao, B.F., Zhou, Y.H., Jiang, S.Q., 2006. Research advances in the Mesozoic tectonic regimes during the formation of Jiaodong ore cluster area. *Prog. Nat. Sci.* 16, 777–784.
- Deng, J., Wang, Q.F., Yang, L.Q., Zhou, L., Gong, Q.J., Yuan, W.M., Xu, H., Guo, C.Y., Liu, X.W., 2008. The structure of ore-controlling strain and stress fields in the Shangzhuang gold deposit in Shandong province, China. *Acta Geol. Sin.* 82, 769–780.
- Deng, J., Yang, L.Q., Gao, B.F., Sun, Z.S., Guo, C.Y., Wang, Q.F., Wang, J.P., 2009. Fluid evolution and metallogenic dynamics during tectonic regime transition: example from the Jiapigou Gold Belt in northeast China. *Resour. Geol.* 59, 140–152.
- Deng, J., Wang, Q.F., Wan, L., Liu, H., Yang, L.Q., Zhang, J., 2011. A multifactorial analysis of mineralization characteristics of the Dayingezhuang disseminated-veinlet gold deposit in the Jiaodong gold province of China. *Ore Geol. Rev.* 40, 54–64.
- Deng, J., Liu, X.F., Wang, Q.F., Pan, R.G., 2015a. Origin of the Jiaodong-type Xinli gold deposit, Jiaodong Peninsula, China: constraints from fluid inclusion and C–D–O–S–Sr isotope compositions. *Ore Geol. Rev.* 65, 674–686.
- Deng, J., Wang, C.M., Bagas, L., Carranza, E.J.M., Lu, Y.J., 2015b. Cretaceous–Cenozoic tectonic history of the Jiaojia Fault and gold mineralization in the Jiaodong Peninsula, China: constraints from zircon U–Pb, illite K–Ar, and apatite fission track thermochronometry. *Mineral. Deposita* 1–20. <http://dx.doi.org/10.1007/s00126-015-0584-1>.
- Dodson, M.H., 1973. Closure temperature in cooling geochronological and petrological systems. *Contrib. Mineral. Petrol.* 40, 259–274.
- Donskaya, T.V., Windley, B.F., Mazukabzov, A.M., Kröner, A., Sklyarov, E.V., Gladkochub, D.P., Ponomarchuk, V.A., Badarch, G., Reichow, M.K., Hegner, E., 2008. Age and evolution of late Mesozoic metamorphic core complexes in southern Siberia and northern Mongolia. *J. Geol. Soc. (London, U.K.)* 165, 405–421.
- Fan, H.R., Hu, F.F., Yang, J.H., Shen, K., Zhai, M.G., 2005. Fluid evolution and large-scale gold metallogeny during Mesozoic tectonic transition in the eastern Shandong province. *Acta Petrol. Sin.* 5, 1317–1328 (in Chinese with English abstract).
- Faure, M., Lin, W., Monié, P., Le Breton, N., Poussineau, S., Panis, D., Deloué, E., 2003. Exhumation tectonics of the ultrahigh-pressure metamorphic rocks in the Qinling orogen in east China: new petrological–structural–radiometric insights from the Shandong Peninsula. *Tectonics* 22 (3), 1–22.
- Galbraith, R.F., 1981. On statistical models for fission track counts. *Math. Geol.* 13, 471–483.
- Galbraith, R.F., 1984. On statistical estimation in fission track dating. *J. Int. Assoc. Math. Geol.* 16 (7), 653–669.
- Galbraith, R.F., Laslett, G.M., 1993. Statistical models for mixed fission track ages. *Nucl. Tracks Radiat. Meas.* 21, 459–470.
- Gao, B.F., 2008. Structural Deformation, Fluid Flow and Gold Mineralization in the Zhaoping Fault Zone, Shandong Province, China (Ph.D. Dissertation), China University of Geosciences, Beijing, China (133 pp. in Chinese with English abstract).
- Gleadow, A.J.W., 1981. Fission-track dating method: what are the real alternatives? *Nucl. Track Detect.* 2, 105–117.
- Goldfarb, R.J., Santosh, M., 2014. The dilemma of the Jiaodong gold deposits: are they unique? *Geosci. Front.* 5 (2), 139–153.
- Goldfarb, R.J., Hart, C.J.R., Davis, G., Groves, D.I., 2007. East Asian gold: deciphering the anomaly of Phanerozoic gold in Precambrian cratons. *Econ. Geol.* 102, 341–346.
- Goldfarb, R.J., Taylor, R.D., Collins, G.S., Goryachev, N.A., Orlandini, O.F., 2014. Phanerozoic continental growth and gold metallogeny of Asia. *Gondwana Res.* 25, 48–102.
- Goss, S.C., Wilde, S.A., Wu, F., Yang, J., 2010. The age, isotopic signature and significance of the youngest Mesozoic granitoids in the Jiaodong Terrane, Shandong Province, North China Craton. *Lithos* 3, 309–326.
- Guedes, S., Moreira, P.A., Devanathan, R., Weber, W.J., Hadler, J.C., 2013. Improved zircon fission-track annealing model based on reevaluation of annealing data. *Phys. Chem. Miner.* 40 (2), 93–106.
- Guo, P., Santosh, M., Li, S., 2013. Geodynamics of gold metallogeny in the Shandong Province, NE China: an integrated geological, geophysical and geochemical perspective. *Gondwana Res.* 24 (3), 1172–1202.
- Hames, W.E., Bowring, S.A., 1994. An empirical evaluation of the argon diffusion geometry in muscovite. *Earth Planet. Sci. Lett.* 124, 161–169.
- Harrison, T.M., Celerier, J., Aikman, A.B., Hermann, J., Heizler, M.T., 2009. Diffusion of ⁴⁰Ar in muscovite. *Geochim. Cosmochim. Acta* 73, 1039–1051.
- Hou, M.L., Jiang, Y.H., Jiang, S.Y., Ling, H.F., Zhao, K.D., 2007. Contrasting origins of Late Mesozoic adakitic granitoids from the northwestern Jiaodong Peninsula, East China: implications for crustal thickening to delamination. *Geol. Mag.* 144, 619–631.
- Hurfurd, A.J., 1986. Cooling and uplift patterns in the Lepontine Alps South Central Switzerland and an age of vertical movement on the Insubric fault line. *Contrib. Mineral. Petrol.* 92 (4), 413–427.
- Hurfurd, A.J., Green, P.F., 1983. The zeta age calibration of fission-track dating. *Isot. Geosci.* 1, 285–317.
- Jahn, B.M., Liu, D.Y., Wan, Y.S., Song, B., Wu, J.S., 2008. Archean crustal evolution of the Jiaodong Peninsula, China, as revealed by zircon SHRIMP geochronology elemental and Nd-isotope geochemistry. *Am. J. Sci.* 308, 232–269.
- Jahn, B.M., Litvinosky, B.A., Zandvilevich, A.N., Reichow, M., 2009. Peralkaline granitoid magmatism in the Mongolian–Transbaikalian Belt: evolution petrogenesis and tectonic significance. *Lithos* 113, 539–541.
- Li, J.W., Vasconcelos, P.M., Zhang, J., Zhou, M.F., Zhang, X.J., Yang, F.H., 2003. ⁴⁰Ar/³⁹Ar constraints on a temporal link between gold mineralization, magmatism, and continental margin transgression in the Jiaodong gold province, Eastern China. *J. Geol.* 111, 741–751.
- Li, J.W., Bi, S.J., Selby, D., Chen, L., Vasconcelos, P., Thiede, D., Zhou, M.F., Zhao, X.F., Li, Z.K., Qiu, H.N., 2012. Giant Mesozoic gold provinces related to the destruction of the North China craton. *Earth Planet. Sci. Lett.* 349, 26–37.
- Lin, W., Wang, Q., 2006. Late Mesozoic extensional tectonics in the North China Block: a crustal response to subcontinental mantle removal? *Bull. Soc. Geol. Fr.* 177, 287–294.
- Lin, W., Chen, Y., Faure, M., Wang, Q.R., 2003. Tectonic implications of new Late Cretaceous palaeomagnetic constraints from Eastern Liaoning Peninsula, NE China. *J. Geophys. Res. Solid Earth* 108 (B6) (EPM 5-1–5-17).
- Lin, W., Faure, M., Monié, P., Schärer, U., Panis, D., 2008. Mesozoic extensional tectonics in Eastern Asia: the South Liaodong Peninsula Metamorphic Core Complex (NE China). *J. Geol.* 116, 134–154.
- Liu, J., Davis, G.A., Lin, Z., Wu, F., 2005. The Liaonan metamorphic core complex, Southeastern Liaoning Province, North China: a likely contributor to Cretaceous rotation of Eastern Liaoning, Korea and contiguous areas. *Tectonophysics* 407, 65–80.
- Liu, Y., Deng, J., Wang, Z.L., Zhang, L., Zhang, C., Liu, X.D., Zheng, X.L., Wang, X.D., 2014a. Zircon U–Pb age, Lu–Hf isotopes and petrogeochemistry of the monzogranites from Xincheng gold deposit, northwestern Jiaodong Peninsula, China. *Acta Petrol. Sin.* 30 (9), 2559–2573 (in Chinese with English abstract).
- Liu, Y., Yang, L.Q., Wang, Z., Zhang, L., Zhang, C., Wang, X.D., 2014b. Petrogeochemistry and geochronology of gold-hosting monzogranites in the Xincheng Gold Deposit, Jiaodong Peninsula, China: implication for gold mineralization. *Acta Geol. Sin. Engl.* 88 (s2), 1646–1647.
- Ma, L., Jiang, S.Y., Dai, B.Z., Jiang, Y.H., Hou, M.L., Pu, W., Xu, B., 2013. Multiple sources for the origin of Late Jurassic Linglong adakitic granite in the Shandong Peninsula, eastern China: zircon U–Pb geochronological, geochemical and Sr–Nd–Hf isotopic evidence. *Lithos* 162, 175–194.
- Marsellos, A.E., Garver, J.L., 2010. Radiation damage and uranium concentration in zircon as assessed by Raman spectroscopy and neutron irradiation. *Am. Mineral.* 95, 1192–1201.
- Maruyama, S., Isozaki, Y., Kimura, G., Terabayashi, M., 1997. Paleogeographic maps of the Japanese Islands: plate tectonic synthesis from 750 Ma to present. *Island Arc* 6, 121–142.
- Mazukabzov, A., Gladkochub, D.P., Donskaya, T.V., Sklyarov, E.V., Ripp, G.S., Izbrodin, I.A., Wang, T., Zeng, L.S., 2011. The Selenga Metamorphic Core Complex (Western Transbaikalian Region). *Dokl. Earth Sci.* 440, 1212–1215.
- McCuaig, T.C., Kerrich, R., 1998. P–T–t–deformation–fluid characteristics of lode gold deposits: evidence from alteration systematics. *Ore Geol. Rev.* 12, 381–453.
- McDougall, I., Harrison, T.M., 1999. *Geochronology and Thermochronology by the ⁴⁰Ar/³⁹Ar method*. Oxford University Press, Oxford.
- Meng, Q.R., 2003. What drove late Mesozoic extension of the northern China–Mongolia tract? *Tectonophysics* 369, 155–174.
- Ni, J., Liu, J., Tang, X., Yang, H., Xia, Z., Guo, Q., 2013. The Wulian metamorphic core complex: a newly discovered metamorphic core complex along the Sulu orogenic belt, eastern China. *J. Earth Sci.* 24, 297–313.
- O’Sullivan, P.B., Parrish, R.R., 1995. The importance of apatite composition and single-grain ages when interpreting fission track data from plutonic rocks: a case study from the Coast Ranges, British Columbia. *Earth Planet. Sci. Lett.* 132 (1), 213–224.
- Passchier, C.W., Trouw, R.A., 2005. *Microtectonics*. 2nd edition. Springer, Berlin, pp. 1–289.
- Qiu, Y.S., 1989. Regional Geological Setting of Gold Deposits in the Zhaoye Gold Belt in Shandong Province. Liaoning Science and Technology Press, Shenyang (in Chinese).
- Qiu, Y., Groves, D.I., McNaughton, N.J., Wang, L.G., Zhou, T., 2002. Nature, age, and tectonic setting of granitoid-hosted, orogenic gold deposits of the Jiaodong Peninsula, eastern North China craton, China. *Mineral. Deposita* 37 (3–4), 283–305.
- Sang, L.K., 1984. The origin and evolution of the Linglong granites. *Earth Sci.* 9, 101–114 (in Chinese).
- Shen, Y.C., Yang, J.H., Liu, T.B., Zeng, Q.D., Li, G.M., 2002. Interlayer-slide – breccia gold deposit—a new type of gold deposit discovered in Jiaodong region. *Geol. Prospect.* 38 (2), 11–14 (in Chinese with English abstract).
- Snee, L.W., Sutter, J.F., Kelly, W.C., 1988. Thermochronology of economic mineral deposits – dating the stages of mineralization at Panasqueira, Portugal, by high precision ⁴⁰Ar–³⁹Ar age spectrum techniques on muscovite. *Econ. Geol.* 83, 335–354.
- Song, M.C., Li, S.Z., Santosh, M., Zhao, S., Yu, S., Yi, P.H., Cui, S.X., Lv, G.X., Xu, J.X., Song, Y.X., Zhou, M.L., 2015. Types, characteristics and metallogenesis of gold deposits in the Jiaodong Peninsula, Eastern North China Craton. *Ore Geol. Rev.* 65, 612–625.
- Spotila, J.A., 2005. Applications of low-temperature thermochronometry to quantification of recent exhumation in mountain belts. *Rev. Mineral. Geochem.* 58 (1), 449–466.
- Sun, W.Z., Li, L., Liu, D.M., Zhang, D.T., Yang, X.F., 2013. Metamorphic Core Complex and Its Controlling Role of Gold Deposits in Western Henan. *Gold* (8), 10–16 (in Chinese with English abstract).
- Tagami, T., Ito, H., Nishimura, S., 1990. Thermal annealing characteristics of spontaneous fission tracks in zircon. *Chem. Geol.* 80, 159–169.
- Vermeesch, P., 2009. RadialPlotter: a Java application for fission track, luminescence and other radial plots. *Radiat. Meas.* 44 (4), 409–410.
- Wagner, G.A., Haute, P., 1992. *Fission-track Dating* vol. 6. Springer Science & Business Media.
- Wang, L.G., Qiu, Y.M., McNaughton, N.J., Groves, D.I., Luo, Z.K., Huang, J.Z., Miao, L.C., Liu, Y.K., 1998. Constraints on crustal evolution and gold metallogeny in the Northwestern Jiaodong Peninsula, China, from SHRIMP U–Pb zircon studies of granitoids. *Ore Geol. Rev.* 13, 275–291.

- Wang, T., Zheng, Y.D., Zhang, J.J., Zeng, L.S., Donskaya, T.V., Guo, L., Li, J.B., 2011. Pattern and kinematic polarity of Late Mesozoic extension in continental NE Asia: perspectives from metamorphic core complexes. *Tectonics* 30 (6), TC6007.
- Wang, T., Guo, L., Zheng, Y., Donskaya, T., Gladkochub, D., Zeng, Li, J., Wang, Y., Mazukabzov, A., 2012. Timing and processes of Late Mesozoic mid-lower-crustal extension in continental NE Asia and implications for the tectonic setting of the destruction of the North China Craton: mainly constrained by zircon U–Pb ages from metamorphic core complexes. *Lithos* 154, 315–345.
- Wang, Z.L., Yang, L.Q., Deng, J., Santosh, M., Zhang, H.F., Liu, Y., Li, R.H., Huang, T., Zheng, X.L., Zhao, H., 2014. Gold-hosting high Ba–Sr granitoids in the Xincheng gold deposit, Jiaodong Peninsula, East China: petrogenesis and tectonic setting. *J. Asian Earth Sci.* 95, 274–299.
- Wang, Z.L., Yang, L.Q., Guo, L.N., Marsh, E., Wang, J.P., Liu, Y., Zhang, C., Li, R.H., Zhang, L., Zheng, X.L., Zhao, R.X., 2015. Fluid immiscibility and gold deposition in the Xincheng deposit, Jiaodong Peninsula, China: a fluid inclusion study. *Ore Geol. Rev.* 65 (3), 701–707.
- Watson, E.B., Harrison, T.M., 2006. Response to comments on “Zircon thermometer reveals minimum melting conditions on earliest Earth”. *Science* 311, 779.
- Wen, B.J., Fan, H.R., Santosh, M., Hu, F.F., Pirajno, F., Yang, K.F., 2015. Genesis of two different types of gold mineralization in the Linglong gold field, China: constraints from geology, fluid inclusions and stable isotope. *Ore Geol. Rev.* 65, 643–658.
- Xu, Y.Q., Lv, G.X., Wang, K., 2013. Characters of alteration, fluid inclusions and mineralization along the detachment fault, Xiadian gold deposit, Jiaodong, China. *Acta Mineral. Sin.* 52, 977–978 (in Chinese).
- Yamada, R., Tagami, T., Nishimura, S., Ito, H., 1995. Annealing kinetics of fission tracks in zircon: an experimental study. *Chem. Geol.* 122 (1), 249–258.
- Yang, Q.Y., Santosh, M., 2015. Early Cretaceous magma flare-up and its implications on gold mineralization in the Jiaodong Peninsula, China. *Ore Geol. Rev.* 65, 626–642.
- Yang, J.Z., Zhao, Y.L., Shen, Y.C., Li, H.M., 2000. Gold mineralization associated with detachment faults in the northeast Jiaolai basin. *Gold Sci. Technol.* 8, 13–20 (in Chinese with English abstract).
- Yang, L.Q., Deng, J., Wang, Q.F., Zhou, Y.H., 2006. Coupling effects on gold mineralization of deep and shallow structures in the northwestern Jiaodong Peninsula, eastern China. *Acta Geol. Sin.* 80, 400–411.
- Yang, L.Q., Deng, J., Ge, L.S., Wang, Q.F., Zhang, J., Gao, B.F., Jiang, S.Q., Xu, H., 2007a. Metallogenic age and genesis of gold ore deposits in Jiaodong Peninsula, eastern China: a regional review. *Prog. Nat. Sci.* 17 (2), 138–143.
- Yang, L.Q., Deng, J., Zhang, J., Wang, Q.F., Gao, B.F., Zhou, Y.H., Guo, C.Y., Jiang, S.Q., 2007b. Preliminary studies of fluid inclusions in Damoqijia gold deposit along Zhaoping fault zone, Shandong province, China. *Acta Petrol. Sin.* 23, 153–160.
- Yang, L.Q., Deng, J., Zhang, J., Guo, C.Y., Gao, B.F., Gong, Q.J., Yu, H.J., 2008. Decrepitation thermometry and compositions of fluid inclusions of the Damoqijia gold deposit, Jiaodong gold province, China: implications for metallogeny and exploration. *J. China Univ. Geosci.* 19, 378–390.
- Yang, K.F., Fan, H.R., Santosh, M., Hu, F.F., Wilde, S.A., Lan, T.G., Liu, Y.S., 2012. Reactivation of the Archean lower crust: implications for zircon geochronology, elemental and Sr–Nd–Hf isotopic geochemistry of Late Mesozoic granitoids from northwestern Jiaodong Terrane, the North China Craton. *Lithos* 146, 112–127.
- Yang, L.Q., Deng, J., Goldfarb, R.J., Zhang, J., Gao, B.F., Wang, Z.L., 2014a. $^{40}\text{Ar}/^{39}\text{Ar}$ geochronological constraints on the formation of the Dayingezhuang gold deposit: new implications for timing and duration of hydrothermal activity in the Jiaodong Gold Province, China. *Gondwana Res.* 25 (4), 1469–1483.
- Yang, L.Q., Deng, J., Wang, Z.L., Zhang, L., Guo, L.N., Song, M.C., Zheng, X.L., 2014b. Mesozoic gold metallogenic system of the Jiaodong Gold Province, eastern China. *Acta Petrol. Sin.* 30 (9), 2447–2467 (in Chinese with English abstract).
- Yang, L.Q., Deng, J., Wang, Z.L., 2014c. Ore-controlling structural pattern of Jiaodong gold deposits: geological–geophysical integration constraints. In: Chen, Y.T., Jin, Z.M., Shi, Y.L., Yang, W.C., Zhu, R.X. (Eds.), *The Deep-seated Structures of Earth in China*. Sciences Press, Beijing, pp. 1006–1030 (in Chinese).
- Yuan, W.M., Zheng, Q.G., Bao, Z.K., Dong, J.Q., Carter, A., An, Y.C., Deng, J., 2009. Zircon fission track thermochronology constraints on mineralization epochs in Altai Mountains, northern Xinjiang, China. *Radiat. Meas.* 44, 950–954.
- Zaun, P.E., Wagner, G.A., 1985. Fission-track stability in zircons under geological conditions. *Nucl. Tracks Radiat. Meas.* 10 (3), 303–307.
- Zhai, M.G., Santosh, M., 2011. The Early Precambrian odyssey of the North China Craton: a synoptic overview. *Gondwana Res.* 20, 6–25.
- Zhang, X.O., Cawood, P.A., Wilde, S.A., Liu, R.Q., Song, H.L., Li, W., Snee, L.W., 2003. Geology and timing of mineralization at the Cangshang gold deposit, Northwestern Jiaodong Peninsula, China. *Mineral. Deposita* 38, 141–153.
- Zhang, J., Zhao, Z.F., Zheng, Y.F., Dai, M., 2010. Postcollisional magmatism: geochemical constraints on the petrogenesis of Mesozoic granitoids in the Sulu orogen, China. *Lithos* 119, 512–536.
- Zhao, L., Zheng, T.Y., Chen, L., Tang, Q.S., 2007. Shear wave splitting in eastern and Central China: implications for upper mantle deformation beneath continental margin. *Phys. Earth Planet. Inter.* 162, 73–84.
- Zhou, X.W., Zhao, G.C., Wei, C.J., Geng, Y.S., Sun, M., 2008. EPMA U–Th–Pb monazite and SHRIMP U–Pb zircon geochronology of high-pressure pelitic granulites in the Jiaobei massif of the North China Craton. *Am. J. Sci.* 308, 328–350.
- Zhu, D.G., Meng, X.G., Ma, Y.S., Shao, Z.G., Feng, X.Y., Qu, W., Zhang, H.P., Fu, H.T., Yang, M.L., Wang, J.P., 2002. Tectonic features of the Yiwuliushan metamorphic core complexes and their controlling to gold deposit in western Liaoning Province. *Geotecton. Metallog.* 26 (2), 156–161 (in Chinese with English abstract).
- Zwingmann, H., Mancktelow, N., 2004. Timing of Alpine fault gouges. *Earth Planet. Sci. Lett.* 223 (3), 415–425.
- Zwingmann, H., Mancktelow, N., Antognini, M., Lucchini, R., 2010. Dating of shallow faults: new constraints from the AlpTransit tunnel site (Switzerland). *Geology* 38 (6), 487–490.